JGR Atmospheres

RESEARCH ARTICLE
10.1029/2023JD038685

Lightning and Radar Characteristics of Tornadic Cells in Landfalling Tropical Cyclones

Benjamin A. Schenkel[1,2,3], Kristin M. Calhoun[2,3], Thea N. Sandmæl[1,2], Zachary R. Fruits[1,3,4], Isaiah Schick[1,3,5], Marcus C. Ake[1,3], and Benjamin F. Kassel[1,3,6]

[1]Cooperative Institute for Severe and High-Impact Weather Research and Operations, Norman, OK, USA, [2]NOAA/OAR National Severe Storms Laboratory, Norman, OK, USA, [3]School of Meteorology, University of Oklahoma, Norman, OK, USA, [4]Now at Texas A&M University, College Station, TX, USA, [5]Now at AccuWeather, Wichita, KS, USA, [6]Now at International Trip Planning Services LLC, Houston, TX, USA

Abstract Tropical cyclone (TC) tornadoes are often associated with lower-skill forecasts compared to midlatitude supercellular tornadoes. Forecasts may be improved through a greater understanding of their lightning and radar signatures. This study investigates the lightning and radar characteristics of TC tornadic cells for comparison with TC non-tornadic cells (i.e., strongly rotating cells without tornadoes) and non-TC tornadic cells using three lightning networks and radar data. These results show that the majority of TC tornadic and non-tornadic cells are not associated with lightning, although the former subset occurs with lightning more often. TC tornadic cases typically have lightning maximized to its northeast, whereas the non-tornadic subset is associated with a lower density of flashes that are more symmetrically distributed. TC tornadic mesocyclones also show stronger low-level rotation and convergence at the time of tornado occurrence compared to non-tornadic cases. Hourly trends in rotation and convergence show stronger increases before tornado occurrence in both variables for TC tornadic mesocyclones, yielding small, nonsignificant differences with non-TC tornadic mesocyclones during tornado occurrence. Finally, analysis of lightning throughout the TC shows that tornadic cells often occur on the downwind edge of a broad lightning maximum, whereas non-tornadic cases occur in the middle of a weaker lightning maximum, with these maxima propagating away from the TC in both subsets.

Plain Language Summary Landfalling tropical cyclones (e.g., tropical storms, hurricanes) often produce tornadoes, which are challenging to forecast. Two factors that may improve these forecasts are lightning and weather radar-derived rotation and convergence data, which have been studied for a limited number of tropical cyclones. Hence, this study investigates the lightning and radar characteristics of tropical cyclone (TC) tornadic cells compared with TC non-tornadic cells (i.e., strongly rotating without tornadoes) and non-tropical cyclone, weakly damaging tornadic cells. These results show that the majority of TC tornadic and non-tornadic cells are not preceded by lightning, although tornadic cells are associated with more lightning more often. Lightning associated with TC tornadic cells is typically located to its northeast, whereas lightning occurs more symmetrically around non-tornadic cells. Low-level rotation and convergence are stronger for TC and non-tropical cyclone tornadic cells at tornado occurrence compared to non-tornadic cases. Finally, tornadic cells tend to occur on the downwind (i.e., in direction of TC wind) edge of a broad-scale lightning maximum, whereas non-tornadic cases occur in the middle of a weaker maximum. These results suggest that trends in radar-derived rotation and convergence may have more value for the real-time identification of tornadoes than lightning.

Key Points:

- Most tropical cyclone (TC) tornadic and non-tornadic cells have no lightning, although tornadic cases have flashes more often to their northeast
- Mesocyclone low-level rotation and convergence increase before TC tornadoes, becoming greater than non-tornadic cases
- Tornadic cells occur closer to the downwind edge of a broader and stronger lightning maximum relative to non-tornadic cells

Supporting Information:

Supporting Information may be found in the online version of this article.

Correspondence to:

B. A. Schenkel,
benschenkel@gmail.com

Citation:

Schenkel, B. A., Calhoun, K. M., Sandmæl, T. N., Fruits, Z. R., Schick, I., Ake, M. C., & Kassel, B. F. (2023). Lightning and radar characteristics of tornadic cells in landfalling tropical cyclones. *Journal of Geophysical Research: Atmospheres*, *128*, e2023JD038685. https://doi.org/10.1029/2023JD038685

Received 9 FEB 2023
Accepted 26 JUL 2023

Author Contributions:

Conceptualization: Benjamin A. Schenkel, Kristin M. Calhoun, Thea N. Sandmæl
Data curation: Benjamin A. Schenkel, Kristin M. Calhoun, Thea N. Sandmæl, Zachary R. Fruits, Isaiah Schick, Marcus C. Ake, Benjamin F. Kassel
Formal analysis: Benjamin A. Schenkel
Funding acquisition: Kristin M. Calhoun
Investigation: Benjamin A. Schenkel, Kristin M. Calhoun, Thea N. Sandmæl, Zachary R. Fruits, Isaiah Schick, Marcus C. Ake, Benjamin F. Kassel
Methodology: Benjamin A. Schenkel, Kristin M. Calhoun, Thea N. Sandmæl
Project Administration: Kristin M. Calhoun

1. Introduction

Tropical cyclones (TCs) frequently produce tornadoes in the 2 days before and after landfall, with some tornadoes occurring up to 7 days after the initial TC landfall (Nowotarski et al., 2021; L. A. Schultz & Cecil, 2009; Edwards, 2012). Although most are associated with sub-significant damage (i.e., ∼93% Enhanced Fujita/Fujita scale ratings of 0–1; Edwards, 2012; McCaul, 1991), TC tornadoes can occasionally cause extensive damage and fatalities, including 3% of all TC-related fatalities in the recent historical record (Rappaport, 2014; L. A. Schultz & Cecil, 2009). Forecasts of TC tornadoes are often less skillful at all lead times compared to non-TC tornadoes (Edwards, 2012; Martinaitis, 2017). These forecasting deficiencies are likely attributable to: (a) ∼88% of TC tornadoes occurring in association with low-topped or miniature supercells, which have been challenging

Resources: Benjamin A. Schenkel, Kristin M. Calhoun
Software: Benjamin A. Schenkel
Supervision: Benjamin A. Schenkel, Kristin M. Calhoun
Validation: Benjamin A. Schenkel
Visualization: Benjamin A. Schenkel
Writing – original draft: Benjamin A. Schenkel
Writing – review & editing: Benjamin A. Schenkel, Kristin M. Calhoun, Thea N. Sandmæl

to explicitly simulate in operational models until recently (Edwards et al., 2012; Jones et al., 2019), (b) their occurrence in high vertical wind shear, low convective available potential energy (CAPE) convective-scale environments with the strongest shear concentrated in the lower troposphere (McCaul, 1991; McCaul & Weisman, 1996), and (c) the large variability in the number of tornadoes spawned among TCs (Edwards, 2012; Schenkel et al., 2020). An examination of the lightning and radar characteristics, and their interrelationship, for cells is warranted as a step toward improving real-time identification. Nontrivial uncertainty remains on whether there are typically increases in lightning, and low-level rotation and convergence in cells before tornado occurrence (McCaul et al., 2004; Spratt et al., 1997, 1998). Prior studies have also yet to examine lightning differences throughout the TC in the hours surrounding the time of tornado occurrence. This incomplete understanding of the kinematic structure of tornadic cells and their associated lightning motivates a systematic examination of a large sample of cases shown here.

The connection among cloud dynamics, microphysics, and electrification is key to understanding the relationship between TC tornadic cells and lightning. Compared to non-TC convection over land, TCs typically produce less lightning, including some cases with nearly no lightning (e.g., 1–2 flashes per hour in Hurricane Hugo (1989); Cecil et al., 2002; Samsury & Orville, 1994). The sometimes infrequent occurrence of lightning in TCs is attributed to only the strongest convection extending well above the freezing level in the warm, moist environment of the TC (Barnes et al., 1983; Marks & Houze, 1987). Charge buildup occurs above the freezing level primarily through the collision of graupel and ice particles in the presence of supercooled water (i.e., non-inductive rebounding charging; Takahashi, 1978; Saunders & Peck, 1998). However, the details of this process differ with distance from the center of a TC due to differences in the depth and concentration of supercooled water (Black & Hallett, 1999; Houze, 2010).

In the deep convection of the eyewall, the graupel and larger ice particles are sufficiently heavy to fall via gravitational sedimentation, whereas lighter ice particles are lofted upwards and outwards by strong, tilted updrafts embedded in the TC transverse circulation. This results in an outward-sloping TC inner-core electric field that only becomes sufficiently strong to produce lightning within the most vigorous eyewall convection (Black & Hallett, 1986, 1999). The remaining convection within the TC inner core is typically organized into rainbands, which tend to be shallow due to subsidence from the eyewall and, hence, are infrequently associated with lightning (Hence & Houze, 2012; Willoughby et al., 1982). This results in the eyewall being a local maximum of both in-cloud (IC) and negative polarity cloud-to-ground (CG) lightning (Corbosiero & Molinari, 2002; Molinari et al., 1999).

In the TC outer region, convection is organized into rainbands that are typically associated with the most lightning in the TC (Cecil et al., 2002; Samsury & Orville, 1994). This outer rain-band lightning maximum is associated with stronger updrafts (Didlake & Houze, 2009; Hence & Houze, 2008), which occur in environments with greater CAPE compared to the inner core and weaker influence of subsidence-induced by eyewall convection (Bogner et al., 2000; Emanuel, 1986). Another contributor to the outer region lightning maximum is the reduction in the horizontal advection of ice and graupel, and the concomitant scavenging of supercooled water by ice (Black & Hallett, 1999; Cecil et al., 2002). This aforementioned factor leads to deeper and higher regions of mixed-phase and frozen hydrometeors that are less strongly sloped with height (Black & Hallett, 1999; Cecil et al., 2002). These conditions lead to enhanced charge separation between graupel and ice particles and, consequently, a greater frequency of IC and negative polarity CG lightning compared to the eyewall (Black & Hallett, 1999; Molinari et al., 1999). The larger CAPE in the TC outer region, concentrated in the lower troposphere, compared to the inner core (Bogner et al., 2000; Molinari et al., 2012) together with strong lower-tropospheric vertical wind shear typically also provides the most favorable kinematic and thermodynamic environments for tornadic convection in the TC (McCaul, 1991; Paredes et al., 2021).

The occurrence of lightning, especially in the deepest convection in TCs, suggests that lightning may be useful to differentiate between non-tornadic and tornadic cases. While prior work has examined the relationship between lightning and tornadoes in non-TC environments, there have only been a limited number of TC studies, which have all primarily focused on 1–2 cases each (McCaul et al., 2004; C. J. Schultz et al., 2011). While lightning is a useful tool for identifying the strongest cells in landfalling TCs, prior work has shown that some cells are associated with little or no lightning before or during a tornado (McCaul et al., 2004; C. J. Schultz et al., 2011). In those cases with lightning, most occurred as IC lightning with only one out 5 of the cells studied preceded by CG flashes (Spratt et al., 1998). When considering only those cases with lightning before TC tornadoes, both total

lightning and CG flash rates were substantially reduced compared to a non-TC subset (McCaul et al., 2004; C. J. Schultz et al., 2009). These smaller flash rates are small enough, such that thresholds for lightning jump algorithms developed for non-TC tornadic cases needed to be lowered to identify TC tornadic cells (L. A. Schultz & Cecil, 2009; C. J. Schultz et al., 2011). Nonetheless, prior work has suggested that TC tornadic cells may be associated with more lightning than their non-tornadic counterparts (McCaul et al., 2004; C. J. Schultz et al., 2011).

The radar signatures of TC mesocyclones also tend to be more marginal than non-TC cases despite being visually and kinematically similar (Edwards et al., 2012; Spratt et al., 1997). Prior work has shown that TC tornadic mesocyclones are characterized by weaker rotational velocities (∼15–35 kt), smaller diameters (2–4 km), shallower rotation depth (≤4 km), and smaller and weaker discrete reflectivity values often ≤50 dBZ (Martinaitis, 2017; Nowotarski et al., 2021; Spratt et al., 1997). TC tornadic mesocyclones occasionally show velocity enhancement signatures (i.e., strong radial velocities above the inflow layer), tornado vortex signatures (i.e., concentrated region of intense rotation), hook echoes, and cycling of rotational velocities, which are traits also observed for non-TC tornadic mesocyclones (Bai et al., 2017; Schneider & Sharp, 2007; Suzuki et al., 2000).In contrast, TC non-tornadic mesocyclones are characterized by weaker rotational velocities, especially at low levels with even larger differences compared to tornadic cells with tornado debris signatures (Nowotarski et al., 2021). However, tornadic and non-tornadic TC mesocyclones may be difficult to categorize based on radar data, leading to high false alarm ratios (Devanas et al., 2008; Martinaitis, 2017).

While prior work has provided a strong foundation for understanding the evolution of TC tornadic cell kinematic and microphysical structure, these studies have focused on a limited number of cases (i.e., 1–6 TCs typically on the lower end of this range; Spratt et al., 1998; Martinaitis, 2017). Hence, a climatology is necessary to examine the relationship among lightning, radar-derived dynamical structure, and TC tornadic cells to test the broader applicability of these studies, especially given their occasional disagreement. This work shows how the frequency and location of lightning and radar-derived low-level rotation and convergence of cells evolve before, during, and after tornadogenesis in a large number of landfalling TCs. This study hypothesizes the following changes in cells in the hour before tornado occurrence: (a) increased lightning and (b) enhanced low-level rotation and convergence. The present study uses a multi-year analysis of tornadic cells in 31 landfalling TCs together with lightning datasets from multiple networks. These data are used to first examine differences in the location and frequency of lightning associated with tornadic and non-tornadic TC cells. Next, differences in radar-derived low-level rotation and convergence from radar among TC tornadic, non-TC tornadic, and non-tornadic TC cells before and during their occurrence are examined. Finally, differences in the location and frequency of lightning before, during, and after tornadic versus non-tornadic cell occurrence are analyzed to understand whether lightning patterns throughout the TC can help discriminate between the two subsets. Following prior work, the term "cell" is defined as the local maximum in reflectivity containing the tornado and its associated mesocyclone, and will be used when referring to lightning. "Mesocyclone" refers to the strongly rotating, small-scale vortex typically associated with the tornado within the broader-scale cell, which will be used when referring to radar-derived low-level rotation or convergence. This study will address the following questions.

1. How do the frequency and location of lightning associated with tornadic and non-tornadic cells differ in TCs?
2. Does lightning increase before tornado occurrence?
3. What differences exist in low-level rotation and convergence before tornado occurrence among TC and non-TC events compared to TC non-tornadic mesocyclones?
4. Are there differences in lightning characteristics throughout the TC before, during, and after tornadic versus non-tornadic cell occurrence?

2. Data and Methods

2.1. TC Data

North Atlantic TC intensity and track data are obtained from the National Hurricane Center HURricane DATa 2nd generation (HURDAT2) archive (Landsea & Franklin, 2013). These data are taken from the International Best Track Archive for Climate Stewardship (IBTrACS), version 4, revision 0 (Knapp et al., 2010). This study examines landfalling TCs, including their post-tropical and extratropical phases, from 2013 to 2020 that produced ≥1 tornado ($N = 31$ TCs). Similar to other data in this study, TC data are temporally interpolated to the time of the start location of the tornado report using a piecewise cubic Hermite polynomial, which preserves the shape

of the time series while not permitting overshoots. The present analysis examines the sensitivity of flashes to the distance of the tornadic cell from the TC center and TC intensity. For the former, terciles of the distribution of tornadic cells are used to categorize tornadic and non-tornadic cells as follows (Ditchek, Molinari, et al., 2019; Rios-Berrios & Torn, 2017): (a) inner (<220 km), (b) middle (220–339 km), and (c) outer radii (>339 km). Similarly, tornadic and non-tornadic cells are categorized into three intensity bins of maximum sustained 10-m wind speed from HURDAT2: (a) tropical depression (≤33 kt), (b) tropical storm (34–63 kt), and (c) hurricane (≥64 kt).

2.2. Tornadic and Non-Tornadic Data

2.2.1. TC Tornadic Cells

In the present study, we examine all TC and non-TC tornado data exclusively associated with a tornado report (i.e., human observed or surveyed; NOAA/National Weather Service NWS, 1950; Edwards & Mosier, 2022). The starting location, time, and maximum damage rating of TC tornadic cells from 2013 to 2020 ($N = 383$ tornadoes) are obtained from the Storm Prediction Center (SPC) TC tornado archive (TCTOR; Edwards & Mosier, 2022). These data have been used in prior studies of TC tornadic supercells (Edwards et al., 2012; Nowotarski et al., 2021). TCTOR is associated with enhanced data reliability resulting from modern reporting and rating practices and the introduction of Next Generation Weather Radar (NEXRAD) radar data (Edwards, 2010; Spratt et al., 1997). Each tornado report has been subjectively analyzed following hurricane season for accuracy and association with a TC (Edwards, 2010; Edwards & Mosier, 2022). However, 2020 data may be particularly uncertain, since site surveys were not conducted by at least some National Weather Service Weather Forecast offices due to the COVID-19 pandemic (R. Deal, personal communication, 8 October 2021). Except for pre-tornadic data (to be discussed later), the analysis of all the tornado data in this study uses the start location and time of the tornado report path. The initial tornado report location is used given the short lifetime of most TC tornadoes as exemplified by a median lifetime of 3 min and 85% of tornadoes existing for <10 min.

Data from 2013 to 2018 have been further quality-controlled using dual-polarization NEXRAD Level-II single-radar data (NOAA National Weather Service Operations Center, 1991; Sandmæl et al., 2023). Each TCTOR tornado report and their associated reports in the National Centers for Environmental Information (NCEI) Storm Events database (NOAA/National Weather Service NWS, 1950) are collocated with a region of strong rotation derived from radar-derived azimuthal shear objects (i.e., the azimuthal derivative of radial velocity quantifying rotation) when within radar range (Sandmæl et al., 2019). For each grid point, the azimuthal shear is computed as the slope of the best-fit line computed using a linear, least squares regression fit to 0.5°-elevation angle radial velocity data in the azimuthal direction along a given radar range, over a 0.75-km azimuthal distance in each direction (Mahalik et al., 2019; Smith & Elmore, 2004). This approach effectively smooths extremes due to radar data quality issues, while considering data within a region that is broader than the neighboring grid points. This study also examines minimum divergent shear data (i.e., the radial derivative of radial velocity quantifying divergence), which is also computed as the slope of the linear least squares fit in the radial direction using data within a 2.5-km radial distance in each direction (Mahalik et al., 2019; Smith & Elmore, 2004).

The radar characteristics of each tornadic mesocyclone within the closest radar scan, are determined by first identifying the mesocyclone location, which is defined as the grid point of maximum azimuthal shear within a 10-km radius and ±90 s of the tornado report (Sandmæl et al., 2023). These strict criteria are imposed to maximize the probability that the cell in the radar scan is currently producing a tornado. The associated maximum azimuthal shear and minimum divergent shear within a 2.5-km radius of the radar-derived location were then recorded, similar to Sandmæl et al. (2023). These radar-derived locations were all manually inspected using single-radar radial velocity and reflectivity to ensure consistency with TCTOR data. The majority of azimuthal shear maxima derived from the radar data were within 2–3 km of the starting tornado location. Any maxima with more egregious disagreement with the TCTOR data were further scrutinized and, if necessary, the SPC and local NWS forecast offices were contacted to potentially resolve these timing and location errors (Sandmæl et al., 2023). Nearly all tornadic and non-tornadic cells in this study are within a 150 km distance of the radar as shown in Figure S2 in Supporting Information S1. This implies that the radar beam is sampling within 3 km of the ground, which is a depth containing most TC tornadic mesocyclones, especially given their shallow depth (Homeyer et al., 2020; McCaul & Weisman, 1996). The distributions of mesocyclone radar range distance among the three subsets are also similar, with a majority of data points ≤100 km from the radar. This threshold is associated with small impacts on calculated versus theoretical azimuthal and divergent shear due to differences in the horizontal

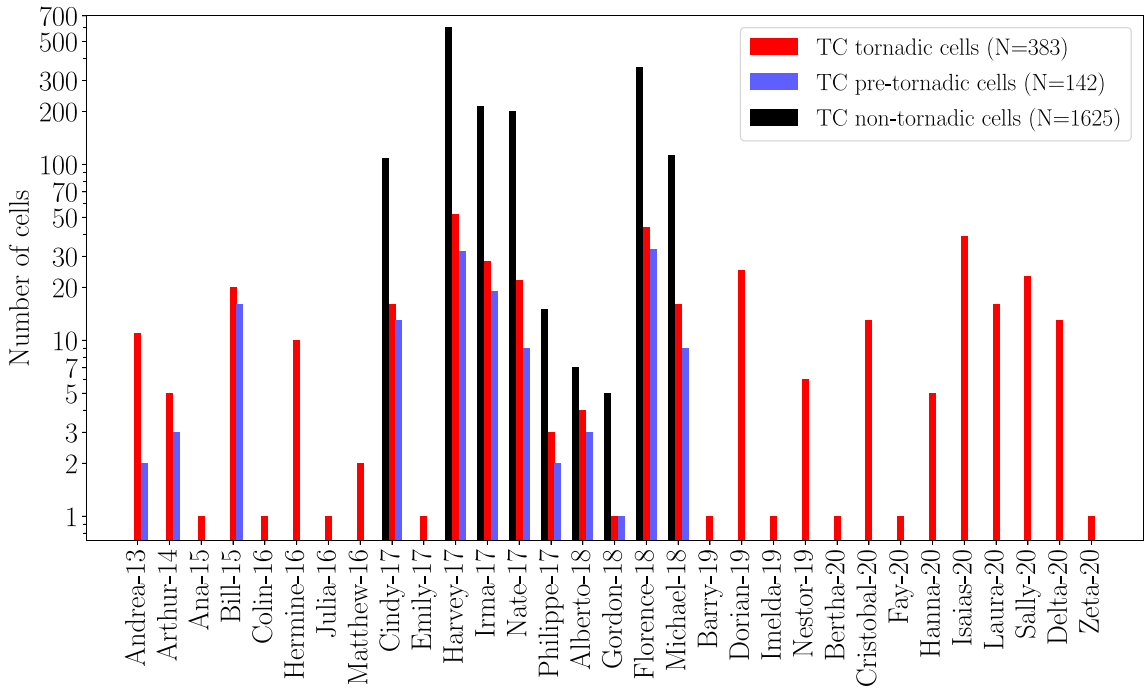

Figure 1. Number of tornadic, pre-tornadic, and non-tornadic cells for each tropical cyclone included in this study.

resolution of the radar beam with distance (Mahalik et al., 2019). Hence, the proximity of the cells to the radar should not strongly impact the results herein. The number of tornadic cells associated with each TC is shown in Figure 1, indicating large inter-storm variability (Edwards, 2012; Schenkel et al., 2020).

2.2.2. TC Non-tornadic Cells

The present analysis uses rotating non-tornadic cells subjectively identified during radar scans of selected TCs where at least one tornadic cell is present from 2017 to 2018 (N = 1625 objects; Sandmæl et al., 2023). Radar scans with at least one tornado are only examined to: (a) identify differences between tornadic and non-tornadic cells similar to what a forecaster does in warning operations and (b) isolate cells in environments that are at least somewhat conducive for tornado occurrence. Strongly rotating cells were manually identified from 0.5°-elevation angle radial velocity and reflectivity data. All cells within ±90 s and a 15-km radius of a tornado report or near the associated tornadic cell track in the hour before the tornado (pre-tornadic to be discussed below) were removed. Hence, this subset does not include any cells before or during tornado reports, but could potentially contain cells after the end time of the tornado report or tornadic cells that were missed in TCTOR due to the occasional challenges of identifying TC tornadoes (e.g., weak tornadoes in remote areas; Edwards et al., 2012; Edwards & Mosier, 2022). Following the method used for the TC tornadic data, the grid point with the maximum azimuthal shear within a 10-km radius of the subjectively identified cell location was assigned as the non-tornadic cell location within the radar scan, similar to Sandmæl et al. (2023). The maximum azimuthal shear and minimum divergent shear within a 2.5-km radius of that location were recorded. Figure 1 shows the number of non-tornadic objects associated with each TC.

2.2.3. Non-TC Tornadic Cells

The radar characteristics of TC tornadic mesocyclones are compared against those from the start location and time of the non-TC tornadic cases obtained from the SPC One Tornado data set (ONETOR; Schaefer & Edwards, 1999). This study only examines EF0 and EF1 non-TC tornadoes (N = 1625), since ≥97% of TC tornadoes fall within these damage rating categories in this study, as shown in prior work (Edwards, 2010, 2012). All non-TC tornado data are excluded whose ONETOR damage rating differs from the maximum damaged-based velocity along the tornado path estimated by the National Weather Service site surveys (~3% of cases; NOAA/National Weather Service NWS, 1950). Despite only including EF0 and EF1 non-TC tornadoes, maximum damage-based velocities are skewed toward slightly weaker, yet significantly different, wind speeds for TC tornadoes with weaker

Table 1
Key Characteristics of the Lightning Detection Networks Used in the Present Study

Network	Sensor type	Lightning type	Study period	Citation
ENTLN	Wideband (waveforms at 1 Hz–12 MHz)	CG, IC	2013–2020	Zhu et al. (2017)
NLDN	Low, very low frequency (waveforms at 400 Hz–400 kHz)	CG, energetic IC[a]	2013–2020	Murphy et al. (2021)
GLM	Optical (solar reflectance at 777.4 nm)	Total lightning[b]	2018–2020	Goodman et al. (2013)

[a]Only CG data from NLDN is used in this study. [b]GLM is unable to determine which flashes are CG versus IC.

median values by 7 mph (as shown in Figure S3 in Supporting Information S1), consistent with 14% more EF0 tornadoes in this subset. This analysis focuses on cases from 2013 to 2018 coinciding with the period in which single radar-derived 0.5°-elevation angle maximum azimuthal shear and minimum divergent shear data have been extracted. The same methodology used to locate and record TC tornado radar characteristics was also followed for the non-TC tornado data (Sandmæl et al., 2023).

2.2.4. Pre-Tornadic Cell Data

This study also uses pre-tornadic data computed by manually tracking cells associated with TC and non-TC tornadoes from 2013 to 2018 backward in time for up to 1 hr by visual examination of radar reflectivity and radial velocity data. Specifically, sequential 0.5°-elevation angle radial velocity and reflectivity data in time are used to identify a first-guess location of the pre-tornadic cell. Each tornadic track point is then centered on the local maximum in 0.5°-elevation angle azimuthal shear data within a 10-km radius of the first guess. The location, time relative to the start of the tornado path, and low-level radar-derived variables within a 2.5-km radius are recorded. These data are used to study trends in radar-derived variables and lightning before the tornado occurs. Figure 1 shows the number of TC tornadic cells with pre-tornadic data ($N = 142$), which is fewer than the number of tornadic cases since not all cases are within radar range or have valid data (e.g., radar beam blockage). Similarly, a subset of non-TC tornadic cells has pre-tornadic data ($N = 908$).

2.3. Lightning Data

This study uses data from three lightning detection networks associated with TC tornadic and non-tornadic data: (a) Earth Networks Total Lightning Network (ENTLN; Liu et al., 2014; Zhu et al., 2017), (b) National Lightning Detection Network (NLDN; Orville, 2008; Cummins & Murphy, 2009; Murphy et al., 2021), and (c) Geostationary Lightning Mapper (GLM; Goodman et al., 2013; Rudlosky et al., 2019). The performance of each network in detecting lightning associated with TC tornadic cells has not been examined for a large sample of cases, which is important given that all three networks are used in operations. We expect the ENTLN to detect the largest number of flashes due to its ability to detect the vast majority of CG and IC lightning. The NLDN and GLM will likely detect fewer flashes since this study only uses CG flashes from the former data set, while the latter is limited by the horizontal resolution of the satellite sensor. More details are included in the text below with key differences summarized in Table 1. A similar analysis of non-TC tornadic cells is excluded in the interest of brevity, as this has been the focus of multiple other studies (e.g., MacGorman, 1993; Stough et al., 2017).

2.3.1. Earth Networks Total Lightning Network

The ENTLN is a wideband (1 Hz–12 MHz) lightning detection network with ≥900 sensors over the continental United States (Liu et al., 2014; Zhu et al., 2017). ENTLN sensors use a time-of-arrival technique to record the time and location of the surge in the electric current (i.e., pulses) associated with each flash. The wave shape and electric field pulse polarity are used to identify the type (i.e., CG vs. IC) and polarity, respectively, of each flash (Zhu et al., 2017). More importantly, the wideband range allows for the detection of both CG and IC lightning (Ringhausen & Bitzer, 2021; Zhu et al., 2017). Flash detection efficiencies are ∼100%, while stroke detection efficiencies are >95% (Zhu et al., 2017). However, regional variations in detection efficiency exist due to heterogeneity in space and time in the sensor network (Bitzer & Burchfield, 2016; Zhu et al., 2017). The present study uses data from 2013 to 2020 coincident with the introduction of ENTLN data. The ENTLN detection efficiency has increased through this period. However, the majority of this data set is post-2017 when the network upgrades were relatively stable, especially for the eastern and southeastern United States. Generally, these changes in detection efficiency likely lead to increased detection of higher flash rate counts during the study period, but do not impact the ability to detect the presence of lightning activity.

2.3.2. National Lightning Detection Network

The NLDN is a wideband (400 Hz–400 kHz) CG and energetic IC lightning detection network with approximately 100 sensors over the continental United States (Murphy et al., 2021). This study uses CG lightning data from the NLDN from 2013 to 2020 for consistency with the availability of the ENTLN data. NLDN sensors use time-of-arrival and magnetic direction finding to determine the location and time of lightning pulses associated with each flash. Detection efficiencies are estimated to be 80%–95% for the ground flashes used in this study (Murphy et al., 2021).

2.3.3. Geostationary Lightning Mapper

The GLM is a charge-coupled device imager aboard the Geostationary Operational Environmental Satellite R-series satellite (Goodman et al., 2013; Rudlosky et al., 2019). This imager is an optical sensor that detects near-infrared emissions at a wavelength of 777.4 nm that are scattered through the cloud tops from lightning flashes. The optical sensor of the GLM can detect both CG and IC flashes (i.e., total lightning) without being able to distinguish between the two (Goodman et al., 2013; Rudlosky et al., 2019). These data are provided every 2 ms on a ∼8 km × ∼8 km horizontal grid at the nadir. Adjacent pixels in space and time with brightness magnitudes above an ambient value are grouped as a single flash and assigned a centroid longitude and latitude (Goodman et al., 2013; Marchand et al., 2019). The detection efficiency of total lightning is ≥ 70% with enhanced detection at night since the optical sensor can more easily identify flashes without the extremely bright background of reflected sunlight during the day (Bateman & Mach, 2020; Zhang & Cummins, 2020). GLM detection efficiencies are also best closest to the nadir of the satellite in the southeastern United States, with greater detection efficiency compared to areas farther north and west (Bateman & Mach, 2020; Marchand et al., 2019).

2.4. Statistical Testing

This study uses a 10,000-sample bootstrap resampling approach for a two-tailed test, with replacement, to quantify differences between distribution statistics including the 5th, 25th, 50th, 75th, and 95th percentiles. Instead of using the 5% level for the testing of the time series or horizontal grids, p-values for local null hypotheses are defined using a false discovery rate with values of $\alpha = 0.1$, corresponding to a global significance level of 5% (Benjamini & Hochberg, 1995). The false discovery rate avoids false rejections of null hypotheses due to random chance or strong spatial autocorrelation by requiring smaller p-values (Wilks, 2016). The number of degrees of freedom is set as the total number of tornadic and non-tornadic data points for each subset. Bootstrapping is used to test differences between: (a) the quantity of lightning between TC tornadic and non-tornadic cells and (b) the maximum azimuthal shear and minimum divergent shear between TC tornadic, TC non-tornadic, and non-TC tornadic cases. This testing both quantifies the uncertainty associated with undersampling the data and the variability associated with each statistic being tested.

3. Results

This study first examines differences in the number and location of flashes between TC tornadic versus non-tornadic cells. Thereafter differences in the low-level radar characteristics of TC tornadic, TC non-tornadic, and non-TC tornadic mesocyclones are analyzed, and how these characteristics vary with the number of flashes. Finally, differences in lightning throughout the TC near the time of the tornadic and non-tornadic cells are studied to understand what differences are potentially unique to each subset.

3.1. Lightning Characteristics of Cells

We first investigate differences in the number of flashes in the 10 min before tornadic and non-tornadic cell occurrence in each of the three lightning networks (Figure 2). Both the majority of tornadic (58%–74% of cases depending on the network) and non-tornadic cells (68%–80%) are not associated with lightning, similar to Spratt et al. (1998). These percentages of cases without lightning are also much larger compared to non-TC tornadic cells shown previously (i.e., ∼0% of cases; Williams et al., 1999; Sandmæl et al., 2019). For the minority of tornadic cells with lightning, the ENTLN shows the highest percentage of cases with ≥1 flash (42% of cases) followed by the GLM (34%) and the NLDN (26%). These results are consistent with the detection efficiencies of these networks and our inclusion of total lightning (e.g., IC and CG) from ENTLN and GLM, and CG data

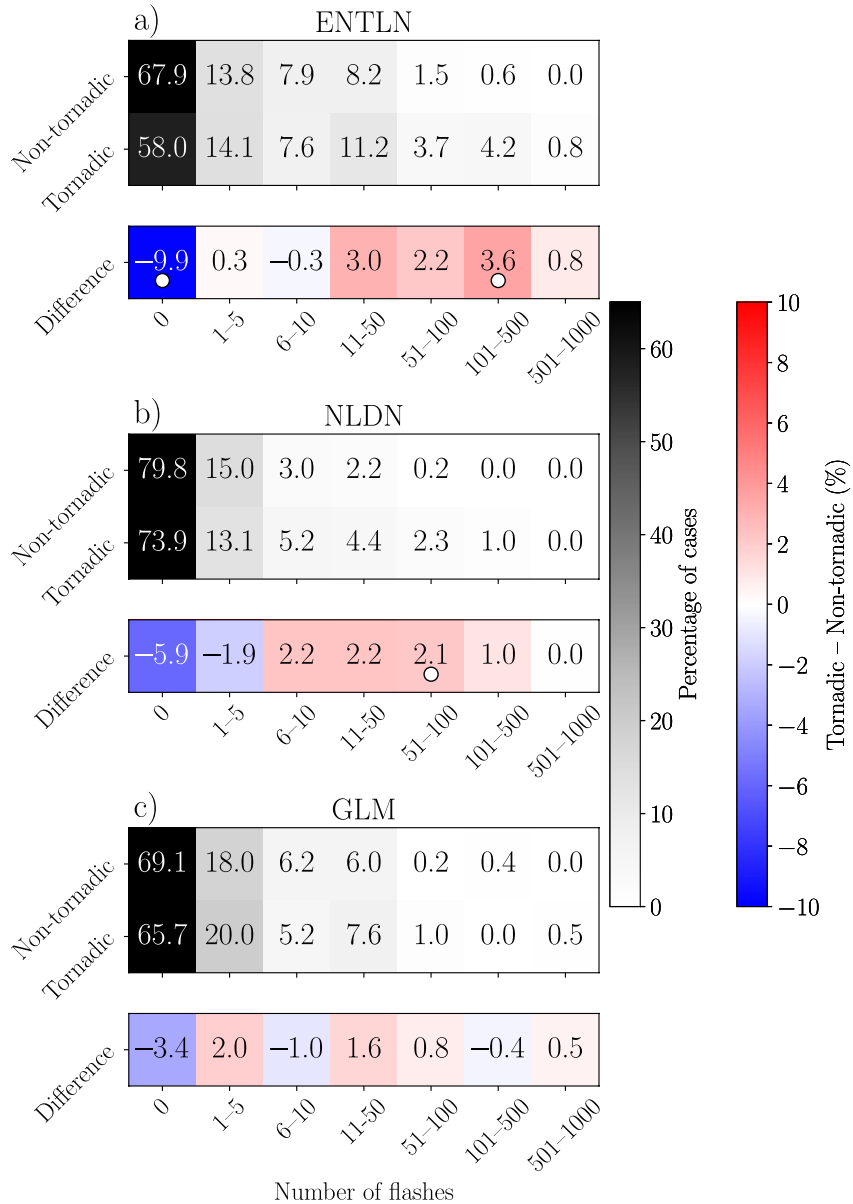

Figure 2. Heat map of flashes (%) within 10 min before and a 10-km radius of tropical cyclone tornadic or non-tornadic cell occurrence and their difference (tornadic-non-tornadic) in the (a) ENTLN, (b) NLDN, and (c) GLM. Boxes with a white dot show statistically significant percentage differences between the tornadic and non-tornadic cells using a 10,000-sample bootstrap test with a false discovery rate of $\alpha = 0.1$.

only from the NLDN (Marchand et al., 2019; Rudlosky et al., 2019). Compared to TC non-tornadic cells, ≥1 flashe occur more frequently for tornadic cases with significantly higher percentages for the ENTLN (10% difference) at $\alpha = 0.1$, which is similar to McCaul et al. (2004). Hence, the strongest difference between tornadic and non-tornadic cells is whether these cells produce any flashes in the ENTLN data, with the caveat being that a minority of cases in both subsets are associated with lightning. The larger differences for ENTLN compared to the NLDN are consistent with the use of only CG flashes from the latter data set and due to most TC lightning occurring as IC rather than CG (Spratt et al., 1998; Willoughby et al., 1985). These facts may also explain the lack of significant differences for most lightning bins (except the 51–100 flash bin) between tornadic and non-tornadic cells in the NLDN. The largest disparities for cases with ≥1 flash between tornadic and non-tornadic cells occur in the distribution extremes at 101–500 flashes for the ENTLN, with differences of 3.6% that are significant at $\alpha = 0.1$. Although not significant, the 501–1,000 flash threshold for the ENTLN may also be useful for

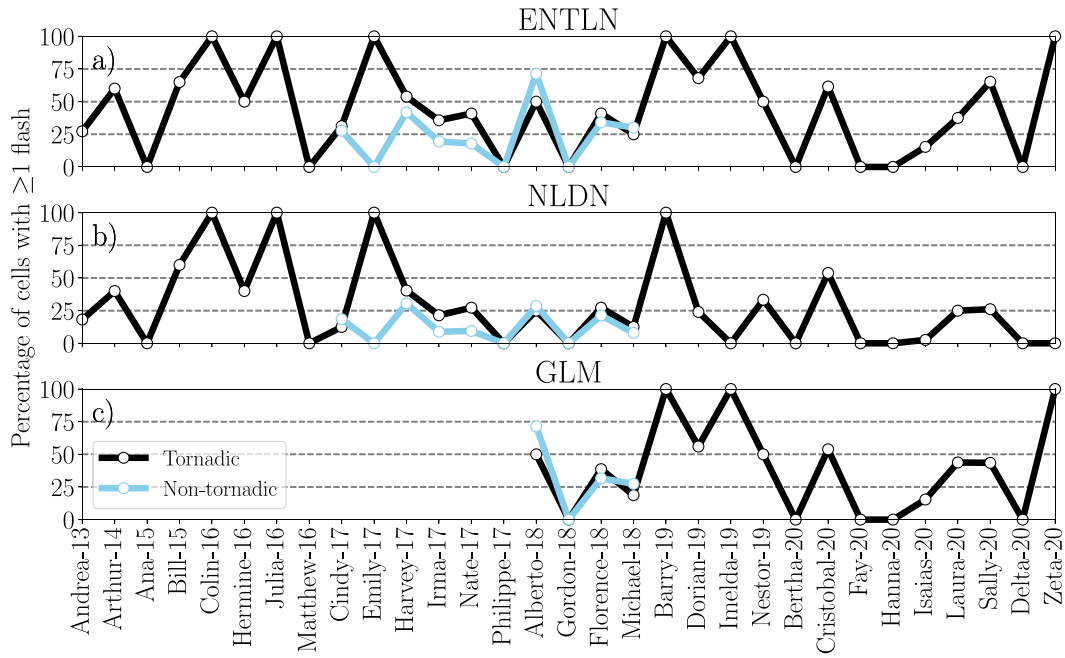

Figure 3. Percentage of tornadic and non-tornadic cells associated with ≥1 flash within 10 min before and a 10-km radius of tropical cyclone (TC) tornadic or non-tornadic cell occurrence, respectively, for the (a) ENTLN, (b) NLDN, and (c) GLM for each TC.

discriminating between tornadic and non-tornadic cells, given the absence of any cases from the latter subset in this bin. The lack of a similar signal in the GLM may be due, in part, to its limitations during periods of enhanced flash rates, which often tend to be associated with flashes with shorter lengths. Hence, this may lead to their classification as a single flash by GLM (Bruning & MacGorman, 2013; Ringhausen & Bitzer, 2021). More broadly, like TC tornadic cells, non-TC tornadic cases also show large variability in the number of flashes before and during the tornado (C. J. Schultz et al., 2011; Williams, 2001).

We next examine the percentage of tornadic and non-tornadic cells with ≥1 flash for each TC (Figure 3). A threshold of ≥1 flash is used here and in the remainder of the study, given the dearth of lightning associated with TC tornadic cells shown in Figure 2 and in prior case studies (McCaul et al., 2004; Spratt et al., 1998). Figure 3 shows that the percentage of tornadic cases with ≥1 flash ranges from 0% to 100% among all networks, similar to the variability shown previously (McCaul et al., 2004; Spratt et al., 1998). The percentage of TC non-tornadic cells shows smaller variability in the fraction of cases with lightning for the ENTLN (0%–71% of cases), NLDN (0%–30%), and GLM (0%–71%). All TCs where no tornadic cells are associated with ≥1 flash occur in cases with small numbers of tornadoes (i.e., less than ≤5; Figure 1). However, the six TCs where all tornadic cells are associated with ≥1 flash also spawn only one tornado each. The top six tornado-producing TCs [that is, Harvey (2017), Irma (2017), Florence (2018), Isaias (2020), Sally (2020)] each spawn at least 23 tornadoes, which are associated with substantial variability in the percentage of tornadoes with lightning including 15%–65%, 3%–40%, and 15%–56% in the ENTLN, NLDN, and GLM, respectively. Non-tornadic cells for these same TCs are associated with similar, albeit smaller percentages with lightning for the subset of cases included in the non-tornadic study period.

We also examine the association of lightning with: (a) distance of the tornadic and non-tornadic cells from the center of the TC and (b) TC intensity at the time of tornadic and non-tornadic cell occurrence as shown in Figures 4a and 4b, respectively. Although other factors were explored based upon prior work (e.g., synoptic-scale deep-tropospheric vertical wind shear, tornado damage rating; Schenkel et al., 2020; Paredes et al., 2021), these factors did not have strong relationships with lightning and are not shown here in the interest of brevity. Figure 4 shows two key results: (a) both tornadic and non-tornadic cells tend to be associated with lightning more frequently as the distance from the TC center increases and (b) tornadic cells in hurricane-strength TCs are associated with lightning more often than non-tornadic cells. Regarding the former point, both tornadic and non-tornadic cells

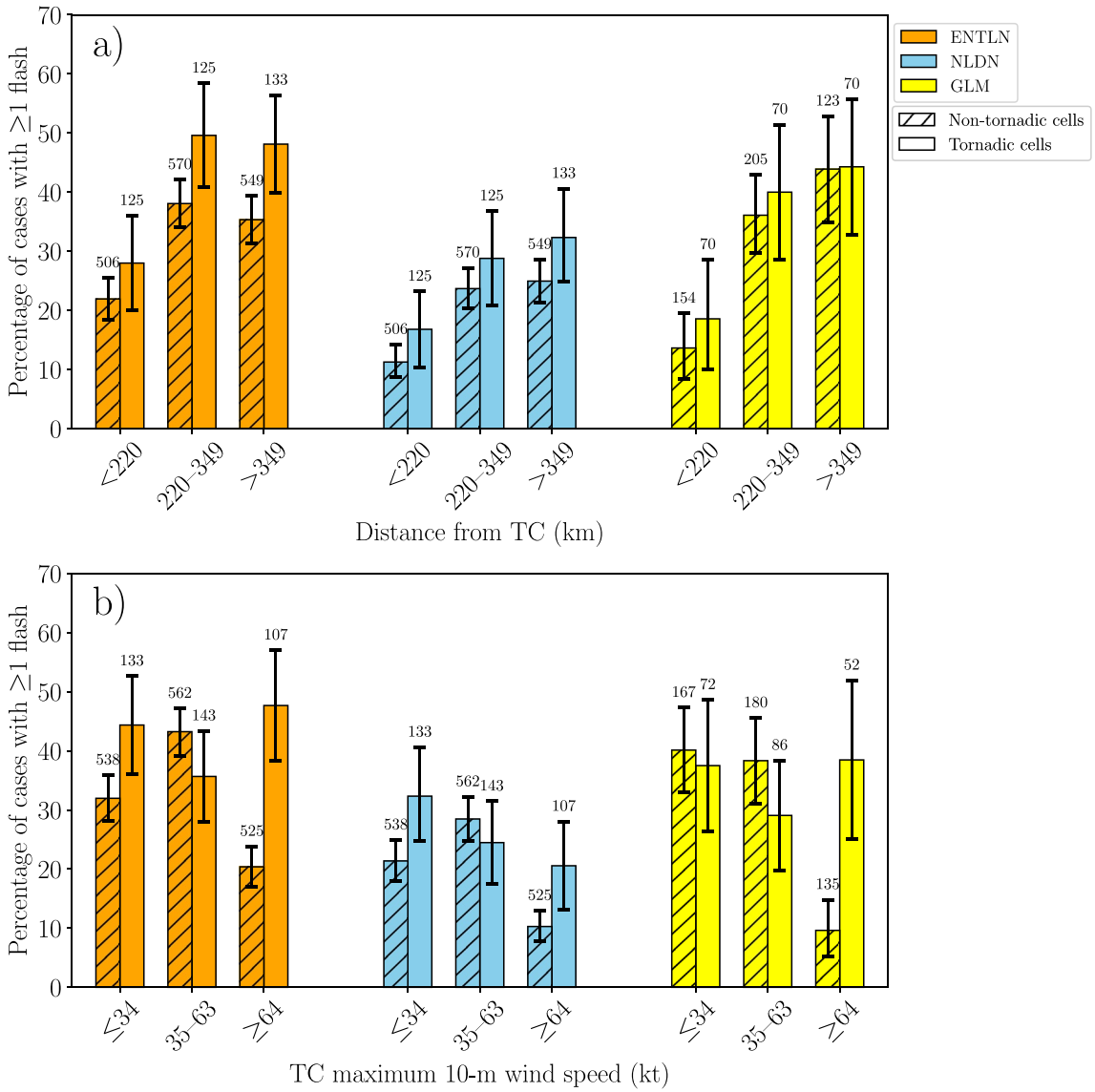

Figure 4. Percentage (bars) and its 95% confidence interval (error bars) computed using a 10,000-sample bootstrap resampling approach of tornadic and non-tornadic cells associated with ≥1 flash within 10 min before and a 10-km radius of tornadic or non-tornadic cell occurrence, respectively, from the ENTLN, NLDN, and GLM subset by (a) distance of the tornadic and non-tornadic cells from the center of the tropical cyclone (TC) (km) and (b) TC intensity (kt) at the time of cell occurrence. The bins for panel (a) are determined from the terciles of the distribution for tornadic cell distance from the TC for all cases in this study. The bins in panel (b) correspond to tropical depression, tropical storm, and hurricane-strength TCs. Sample sizes are shown for each subset above the bars.

in the bin farthest from the center (25%–48% of cases) are associated with a significantly larger number of cases with ≥1 flash at the 5% level compared to those at inner radii (11%–28%) among all three networks. This result may be due to increased CAPE, reduced scavenging of supercooled water, and weaker subsidence associated with the TC secondary circulation at outer radii (Black & Hallett, 1999; Bogner et al., 2000; Emanuel, 1986). However, distance from the center is not a strong discriminant between non-tornadic and tornadic cells with only the ENTLN showing significant differences at the 5% level between the two subsets in the outermost bin.

In contrast to distance from the TC center, TC intensity shows no systematic relationship with lightning in TC tornadic and non-tornadic cases among bins (Figure 4b). Nonetheless, a significantly larger percentage of tornadic cells in hurricane-strength TCs (21%–48%) at the 5% level tend to be associated with ≥1 flash compared to non-tornadic cases (10%–20%). This difference is primarily associated with a significant reduction in the percentage of non-tornadic cells with lightning in hurricanes compared to the weaker TC intensity bins. These large differences in hurricanes may be due to their stronger secondary circulation and associated subsidence outside

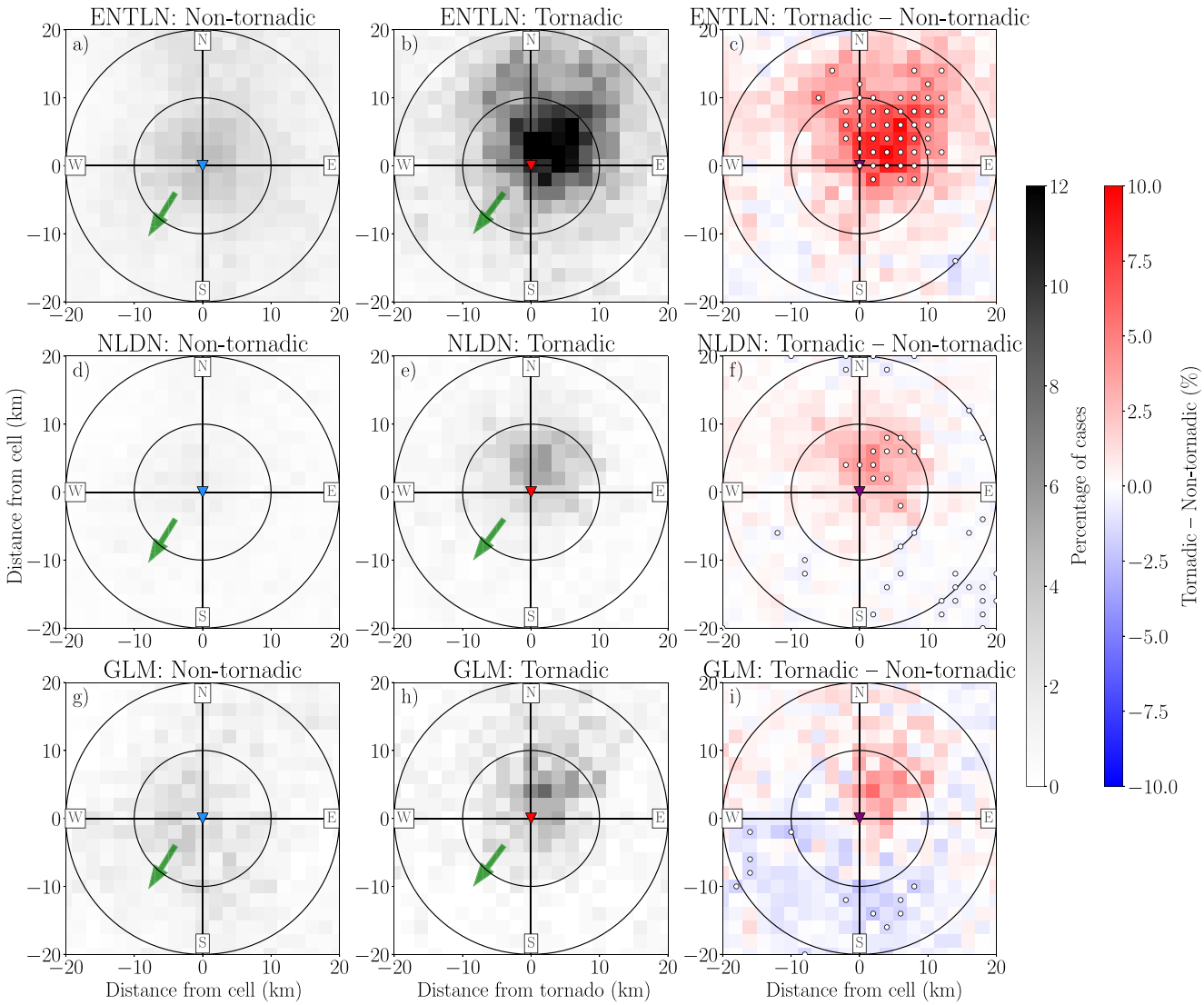

Figure 5. Percentage of cases on a 2-km × 2-km grid with ≥1 flash within 10 min before (a, d, and g) non-tornadic, (b, e, and h) tornadic cells, and (c, f, and i) their difference (tornadic-non-tornadic cells) shown relative to tornadic or non-tornadic cell location for the (a–c) ENTLN, (d–f) NLDN, and (g–i) GLM. The azimuthal reference frame is relative to North, which is pointing up. The triangle at the plot center denotes the location of the tornadic or non-tornadic cell. Range rings are shown every 10 km. The green vector points to the composite median direction of the tropical cyclone center relative to the cell. The small white circles denote bins with statistically significant percentage differences between the tornadic and non-tornadic subsets using a 10,000-sample bootstrap test with a false discovery rate of $\alpha = 0.1$ in panels (c, f, and i).

the eyewall that attempts to reduce the depth of updrafts, such that only the strongest cells have a sufficiently deep mixed-phase region for lightning production (Emanuel, 1986; Hence & Houze, 2012). Considering the distance from the TC center and TC intensity jointly shows even greater differences, with 62% of tornadic cells associated with ≥1 flash compared to 24% of non-tornadic cases at outer radii in hurricanes (not shown here). Even so, the sample size of TC tornadic cells in this subset is small ($N = 13$), suggesting that this result could be an artifact of undersampling.

Next, Figure 5 shows large differences in the cell-relative location of flashes between TC tornadic and non-tornadic cases. The shading of each grid box in Figure 5 represents the percentage of cases with ≥1 flash within 10 min of the TC tornadic or non-tornadic cell. TC tornadic cases have lightning concentrated to the northeast with maximum grid point values of 14%, 6%, and 8% in the ENTLN, NLDN, and GLM, respectively. This location did not change when considering lightning in the hour before the tornado (not shown). Prior case studies have also shown a lightning maximum to the northeast of TC tornadic cells (Spratt et al., 1998). This maximum to

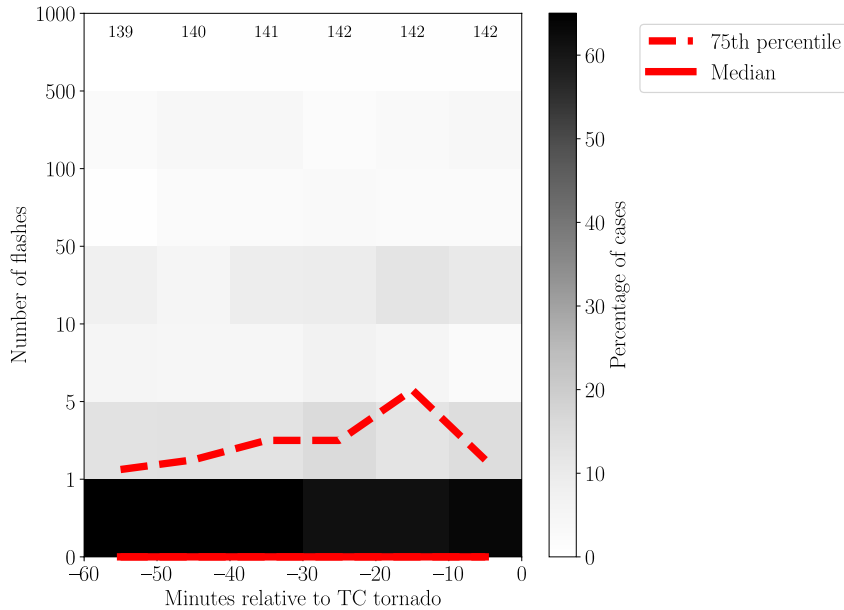

Figure 6. Joint histogram of ENTLN flashes within a 10-km radius versus minutes relative to the tornado using the same *y*-axis scaling for lightning from Figure 2. The median and 75th percentile are not significantly different from zero in this plot or throughout the time series compared to its values at 50–60 min before the tornado. The numbers at the top of each joint histogram bin show the sample size for each 10-min interval. None of the bins show statistically different values compared to those in the 50–60-min bin, as tested using a 10,000-sample bootstrap test with a false discovery rate of $\alpha = 0.1$.

the northeast is consistent with the typical tilt of convection away from the TC center with height, in the direction of the TC outflow, given that most cells occur to the northeast of the TC (see green vector in Figure 5), consistent with prior work (Baker et al., 2009; Eastin & Link, 2009). This is due to most flashes occurring within the anvil, similar to non-TC cases (Ray et al., 1987; Spratt et al., 1998). However, there also exists nontrivial variability in the location and magnitude of the lightning maximum with the TC-relative azimuth and distance from the TC center of the cells (not shown). This is partially due to the direction of the TC advective winds and, hence, the convective outflow changing with TC-relative azimuth, which includes variations in the direction of the: (a) convergent, cyclonic advective winds of the TC primary circulation and (b) the divergent, anticyclonic radial outflow of the TC secondary circulation (Barnes et al., 1983; Barron et al., 2022; Hence & Houze, 2008). Moreover, TC outer radii are also characterized by a deeper mixed phase region with greater concentrations of supercooled water due to increased CAPE, reduced scavenging of supercooled water, and weaker subsidence associated with the TC secondary circulation (Black & Hallett, 1999; Molinari et al., 2012). In contrast, non-tornadic cells are associated with less frequent lightning, as shown by grid point maxima of 5%, 2%, and 4% in the ENTLN, NLDN, and GLM, respectively, with flashes distributed more symmetrically. A comparison of tornadic and non-tornadic subsets shows that the most significant differences are to the northeast. However, a secondary area of significant differences at $\alpha = 0.1$ is broadly scattered in the southern half of the grid that may be related to suppressed lightning in the tornadic cells for the NLDN and GLM.

Finally, trends in flashes in the hour before the TC tornado are shown in Figure 6. There remain small increases in the percentage of cases with 51–100 flashes and ≥501 flashes, and in the 75th percentile during the hour before the tornado. However, none of these increases are significant at $\alpha = 0.1$ for the median, interquartile range, or any of the individual grid boxes. These results likely reflect the lack of lightning in the hour before the tornado. However, there is substantial case-to-case variability, especially among TC tornadic cases with large numbers of flashes before tornado occurrence (i.e., ≥51 flashes per 10 min), suggesting that rapid increases in lightning may occasionally occur as suggested by prior work (C. J. Schultz et al., 2009, 2011).

These results show that most TC tornadic and non-tornadic cells are not associated with lightning in the hour before their occurrence, although there is substantial variability in cases within the former subset. However, flashes occur more frequently with tornadic cases, especially in large numbers within the ENTLN given its detection of a larger number of IC and CG pulses compared to the GLM and NLDN. Flashes also tend to be more

concentrated to the northeast of the tornadic subset compared to non-tornadic cases, which are more symmetrically distributed. There is also substantial variability in the percentage of tornadic and non-tornadic cells with lightning among TCs, which may be related to differences in their location in the TC as well as TC intensity. As an example, Hurricane Ivan (2004) spawned few tornadoes at inner radii, despite producing the most tornadoes in the modern historical record ($N = 118$ tornadoes; Edwards, 2012; Carroll-Smith et al., 2019).

3.2. Radar Characteristics of Cells

In contrast to lightning, the radar characteristics of TC tornadic mesocyclones differ from non-TC EF0-1 tornadic and TC non-tornadic subsets as shown in distributions of 0.5°-elevation angle maximum azimuthal shear (Figure 7a) and minimum divergent shear (i.e., maximum convergent shear; Figure 7b). All three distributions are approximately lognormal with positive skewness for maximum azimuthal shear and negative skewness for minimum divergent shear. The TC tornadic distribution is strongly shifted toward more positive azimuthal shear and negative divergent shear compared to TC non-tornadic cases as indicated by significant differences at the 5% level for the 5th, 25th, 50th, 75th, and 95th percentiles of the two distributions, similar to previous work (Martinaitis, 2017; Nowotarski et al., 2021). The stronger magnitudes of azimuthal and divergent shear for non-TC tornadoes are consistent with stronger maximum damage-based velocity estimates derived from damage indicators (Figure S3 in Supporting Information S1; Edwards et al., 2013; NOAA/National Weather Service NWS, 1950), and a smaller percentage of EF0 tornadoes (56% of non-TC tornadoes are EF0) relative to TC tornadoes (70% are EF0), consistent with previous studies (L. A. Schultz & Cecil, 2009; Edwards, 2012). Median values of the maximum azimuthal shear values for TC tornadic mesocyclones (10.3×10^{-3} s^{-1}) are over two times larger compared to TC non-tornadic mesocyclones (4.8×10^{-3} s^{-1}), whereas median minimum divergent shear values are ∼70% larger (-7.0×10^{-3} s^{-1} vs. -4.0×10^{-3} s^{-1}). However, some overlap remains consistent with the challenges of discriminating between the two subsets in real time as has been discussed previously (Devanas et al., 2008; Martinaitis, 2017).

Contrasting TC tornadic with non-TC tornadic mesocyclones shows the upper half of the non-TC distribution is shifted toward larger magnitudes for both azimuthal and divergent shear, as supported by significant differences, at the 5% level, for the 95th and 75th percentiles. However, these differences are much smaller compared to those between TC tornadic and non-tornadic mesocyclones as exemplified by a comparison of median azimuthal shear for non-TC tornadic (11.0×10^{-3} s^{-1}), TC tornadic (10.3×10^{-3} s^{-1}), and TC non-tornadic mesocyclones (4.8×10^{-3} s^{-1}). These small disparities between non-TC tornadic and TC tornadic subsets are expected, given the typically weaker low-level rotation and convergence of TC miniature mesocyclones compared to non-TC cases (McCaul, 1987; McCaul & Weisman, 1996).

Next, differences in maximum azimuthal and minimum divergent shear in the hour before the tornado for TC and non-TC cases are compared (Figure 8). Both subsets show azimuthal and divergent shear that are clustered near weaker values initially, followed by a shift and broadening of the distribution toward stronger values, especially in the 30 min before the tornado. The 25th, 50th, and 75th percentiles each become statistically greater than their initial values at 20–40 min before the tornado for TCs and 30–40 min before for non-TC cases at $\alpha = 0.1$ as suggested by prior work (Sandmæl et al., 2019; C. J. Schultz et al., 2009). Comparison of TC and non-TC tornadic mesocyclones shows that the upper extreme of the non-TC tornadic azimuthal shear distribution is slightly shifted toward stronger values, as shown by significant differences between the two histograms in Figure 8e and the 75th percentile in Figure 8c. However, these small differences lessen with time, such that only the strongest azimuthal shear bin consistently shows differences between TC and non-TC tornadic subsets in the 30–40 min before the tornado. This result suggests a slightly quicker broadening of the TC mesocyclone distribution to include stronger values, consistent with their shorter life cycle (McCaul, 1987; Spratt et al., 1997). The smaller sample sizes of pre-tornadic data for both subsets (Figure 1) make it harder to reject the null hypothesis for statistical testing, which partially explains the differing conclusions from Figure 7 especially given its significant, yet small, differences in magnitude.

Similar differences are also observed between the TC and non-TC minimum divergent shear distributions including statistically stronger values, at $\alpha = 0.1$, compared to their initial values. Specifically, these disparities begin slightly earlier for minimum divergent shear compared to maximum azimuthal shear. Differences between the tornadic and non-tornadic subsets also remain until closer to the start of the tornado track (that is, –(30–20) min prior) for the 25th percentile and, to a lesser extent, the median compared to the 75th percentile for maximum azimuthal shear.

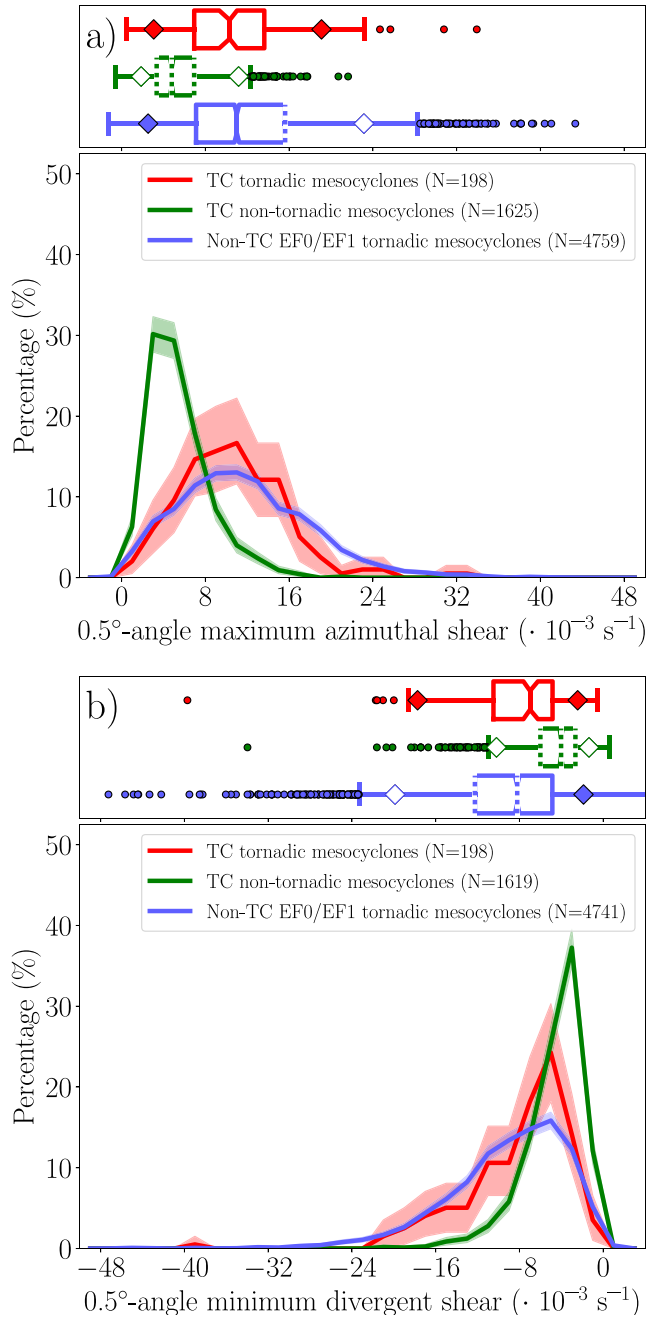

Figure 7. Histogram and box-and-whiskers plot showing 0.5°-elevation angle (a) maximum azimuthal shear (· 10^{-3} s^{-1}) and (b) minimum divergent shear (· 10^{-3} s^{-1}) for tropical cyclone (TC) tornadic, TC non-tornadic, and non-TC EF0–1 tornadic mesocyclones. The shading for each distribution shows its 95% confidence interval computed from a 10,000-sample bootstrap approach with replacement. The box plots show the median (vertical line near box center) and its 95% confidence interval calculated from a 10,000-sample bootstrap approach with replacement (notches on boxes), the interquartile range (box perimeter; (q_1, q_3)), the whiskers (capped lines), and the 5th and 95th percentiles (diamonds). The lower whisker is the first datum above q_1–1.5(q_3–q_1), and the upper whisker is the first datum below q_3 + 1.5(q_3–q_1). Dotted lines in the box-and-whiskers over the median, 25th, or 75th percentiles indicate when these statistics are significantly different from the TC tornadic subset statistics at the 5% level, while white-filled diamonds are used to show significant differences for the 5th or 95th percentiles.

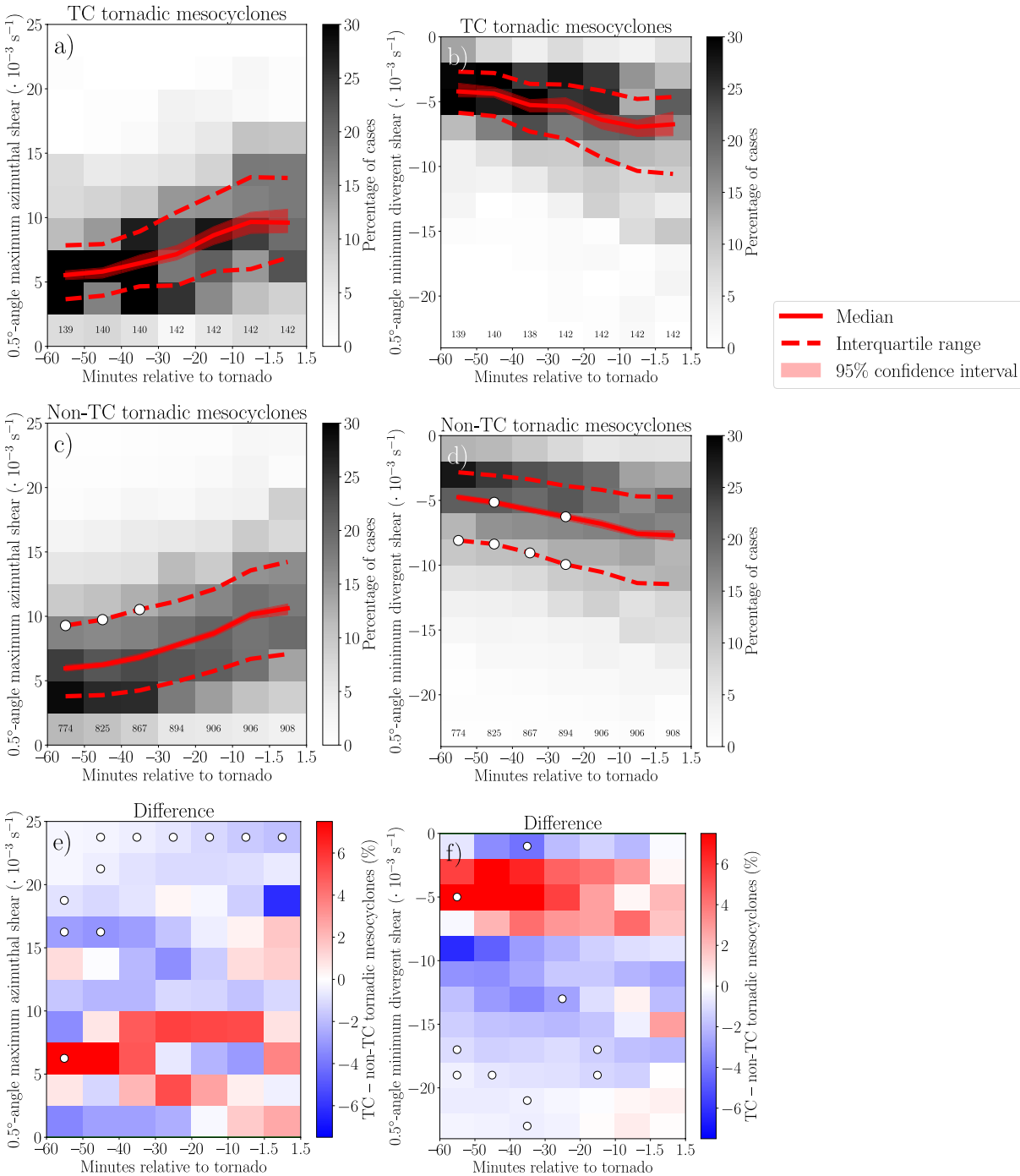

Figure 8. Joint histogram of minutes relative to the tornado versus (a, c, and e) 0.5°-elevation angle maximum azimuthal shear (· 10^{-3} s^{-1}) and (b, d, and f) 0.5°-elevation angle minimum divergent shear (·10^{-3} s^{-1}) for (a and b) tropical cyclone (TC) tornadic, (c and d) non-TC tornadic mesocyclones, and (e and f) their difference (TC tornadic-non-TC tornadic mesocyclones). The percentages are calculated relative to the total number of points within each time bin with the sample size of each bin written near the bottom of the *y*-axis. The white circles in panels (c and d) denote significant differences between the TC tornadic and non-TC tornadic cases for either the 25th, 50th, or 75th percentiles using a 10,000-sample bootstrap test with a false discovery rate of $\alpha = 0.1$. The white circles in panels (e and f) show grid boxes with significant differences between the TC tornadic and non-TC tornadic subsets.

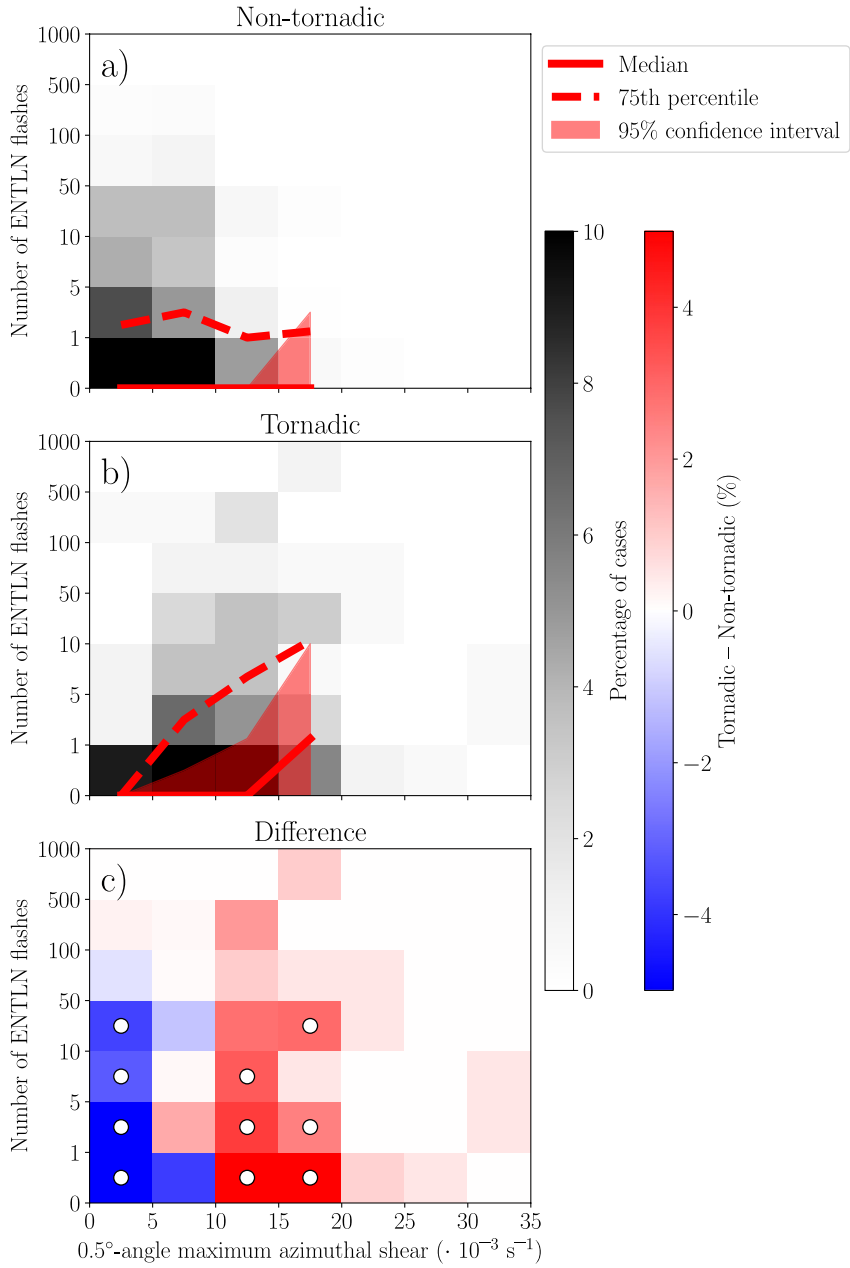

Figure 9. Joint histogram of 0.5°-elevation angle maximum azimuthal shear ($\cdot 10^{-3}$ s^{-1}) versus the number of ENTLN flashes within 10 min before and a 10-km radius of tropical cyclone (a) non-tornadic, (b) tornadic cells, and their (c) difference (tornadic-non-tornadic cells). White circles denote bins with statistically different percentages between the tornadic and non-tornadic subsets using a 10,000-sample bootstrap test with a false discovery rate of $\alpha = 0.1$ in panel (c).

Figure 9 shows that no relationship exists between the number of flashes and the maximum azimuthal shear for TC tornadic and non-tornadic subsets to more strongly link the analysis of lightning and radar-derived kinematic variables shown previously. This is especially important, given the uncertainties with identifying TC tornadoes and their damage rating (Edwards, 2012; Edwards et al., 2012). For simplicity, the analysis here and in the remainder of the study focuses on the ENTLN given its higher detection efficiencies compared to the other networks. The results for maximum azimuthal shear are also similar to minimum divergent shear, which are not shown in the interest of brevity. Both TC non-tornadic and tornadic cases show that stronger low-level rotation is not typically associated with more lightning as supported by 25th, 50th, and 75th percentiles, which are not statistically greater than 0 flashes at $\alpha = 0.1$ for any maximum azimuthal shear bin. These results are also consistent

with the lack of differences in lightning between TC tornadic cells in different damage-rating categories (i.e., EF0 vs. EF1; not shown), and are also similar to prior case studies (McCaul et al., 2004; Spratt et al., 1998).

Comparison of tornadic and non-tornadic cases shows two sources of significant differences (Figure 9c): (a) non-tornadic cases are associated with a greater range in the number of flashes compared to their tornadic counterparts in the weakest azimuthal shear bin and (b) tornadic cells are more frequently associated with stronger low-level rotation relative to non-tornadic cases yielding differences in the 10–20 $\times$ 10^{-3} s^{-1} bins. Regarding the second point, there are a limited number of tornadic cells with both strong rotation and large numbers of flashes associated with significant differences across a wide variety of flash thresholds. The lack of a strong relationship between lightning and low-level rotation in cells is consistent with the lack of increasing flashes before tornadoes (Figure 6) despite strengthening low-level rotation and convergence (Figure 8), similar to previous studies (McCaul et al., 2004; Spratt et al., 1998). This result may be attributed to variability in the height of the supercell, with even cells at TC outer radii failing to extend about the freezing level despite CAPE often being greater at these distances (Bogner et al., 2000; Morotomi et al., 2020). This variability in cell height relative to the freezing level, even at outer radii, may occur due to strong differences in convective-scale buoyancy and vertical wind shear environments of cells that depend on TC structure and its interaction with its synoptic-scale environment (e.g., the existence of shear-or buoyancy-limiting boundaries; Edwards & Pietrycha, 2006; Green et al., 2011).

These results suggest significant increases in low-level rotation and convergence starting up to 40 min before the tornado for TC and non-TC mesocyclones. However, these increases in low-level rotation and convergence are not typically associated with increased lightning flashes. Hence, these results suggest that radar-derived quantities may be a more useful discriminant for identifying tornadic versus non-tornadic mesocyclones in TCs compared to lightning similar to prior work (Martinaitis, 2017; McCaul et al., 2004). However, even tornadic mesocyclones within the same TC rainband may show substantial differences in rotation and other radar characteristics (e.g., with and without hook echoes) presenting challenges in identifying tornadoes (Baker et al., 2009; Devanas et al., 2008). This is consistent with the marginal structure of the associated miniature supercells (Edwards et al., 2012; McCaul & Weisman, 1996), potentially necessitating finer spatiotemporal radar data like those from a phased array radar (Adachi & Mashiko, 2020; Morotomi et al., 2020).

3.3. Lightning Characteristics of TCs

Rather than focusing on lightning associated with the tornadic or non-tornadic cells, this last subsection examines the spatiotemporal evolution of lightning throughout the TC before and after tornadic and non-tornadic cell occurrence, with a focus on scales much broader than the cells. This larger-scale focus may be useful especially when lightning data are available and radar data are sparse given that prior work has shown that: (a) most tornadoes occur in TC outer rainbands, which often have prodigious numbers of flashes (Edwards et al., 2012; Molinari et al., 1999), and (b) the downwind side of the convective portion of TC rainbands tends to have the most intense cells suggesting a preferred location of tornadic supercells (Hence & Houze, 2008, 2012). The dissimilarities in lightning throughout the TC between the two subsets shown here may be largely driven by the latter factor, with the median TC-relative azimuth of tornadic cells rotated 15° counter-clockwise compared to non-tornadic cells (Figure S1 in Supporting Information S1), which corresponds to a median separation distance of 91 km. This 15° angular separation is large relative to the ≤45° TC-relative azimuthal range of the broader scale lightning maxima that these cells are embedded within (to be shown). Moreover, the scale of this horizontal separation distance can also be associated with large differences in the region of the TC, and associated convective-scale environments, that tornadic versus non-tornadic cells are located within (e.g., inner vs. outer rain bands, TC-relative northeast vs. southeast quadrant; Barnes et al., 1983; Hence & Houze, 2008; Schenkel et al., 2020). However, Figure S1 in Supporting Information S1 may give the appearance of a stronger overlap between the two subsets due to the coarse grid box size used to reduce noise. Additionally, most of the results shown in this section, unless otherwise noted, are not artifacts of the different groups of TCs included in tornadic versus non-tornadic cell subsets (not shown).

Differences in lightning throughout the TC exist between tornadic and non-tornadic cells as is evident using a heat map on a TC-relative rectangular grid (Figure 10). These plots use a TC tornadic or non-tornadic cell-relative azimuthal coordinate, such that the TC-relative azimuthal location of each cell has been rotated to be to the right of the TC with the flashes at the time of each cell rotated by the same angle to retain their cell-relative location. The azimuth to the right of the TC is chosen due to climatological preference for tornadoes to occur on the eastern

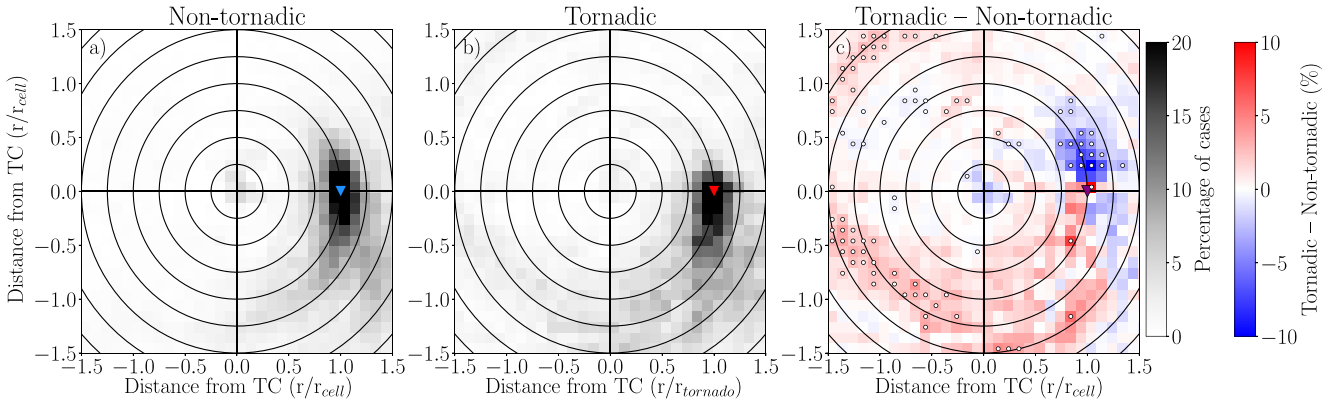

Figure 10. Percentage of cases with ≥1 ENTLN flashes on a $0.1r/r_{cell} \times 0.1r/r_{cell}$ rectangular grid normalized by the TC-relative distance of (a) non-tornadic, (b) tornadic cells, and (c) their difference (tornadic-non-tornadic cells). The location of each tornadic or non-tornadic case and flash have been rotated around the tropical cyclone, such that the cell is always located to the right, as shown by the triangles. The radial coordinate is normalized by the TC-relative distance of each cell, such that the cell is always located at $r/r_{cell} = 1$. White circles show bins with statistically significant percentage differences between the tornadic and non-tornadic subsets using a 10,000-sample bootstrap test with a false discovery rate of $\alpha = 0.1$ in panel (c).

half of the TC (Hill et al., 1966; Novlan & Gray, 1974). These plots also use a radial coordinate normalized by the TC-relative distance of the tornadic or non-tornadic cell, such that each cell is located at $r/r_{cell} = 1$. Hence, all cells in each subset are located to the right of the TC at $r/r_{cell} = 1$ to help isolate differences in lightning despite the differing TC-relative azimuths and distances between the two subsets (i.e., Figure S1 in Supporting Information S1 of the supplement). To facilitate a more direct comparison with the TC tornado start location and time, TC non-tornadic cells in this section are limited to those with maximum azimuthal shear values $\geq 9.0 \times 10^{-4}$ s^{-1} ($N = 1{,}610$ non-tornadic cases), which corresponds to the threshold associated with the 1st percentile for severe weather reports (Sandmæl et al., 2023).

Figure 10 indicates that TC tornadic cells are typically located in the downwind edge (i.e., in the direction of lower-tropospheric cyclonic TC winds) of a lightning maximum with maximum grid point values of 49%. Grid boxes showing lightning in ≥15% of cases wrap along a ≤45° TC-relative azimuth and a narrow set of TC-relative radii. Non-tornadic cells are located near the middle of a weaker lightning maximum with comparatively lower maximum grid point values of 40%. These differences in the location and magnitude of lightning between the tornadic and non-tornadic subsets are significant at $\alpha = 0.1$ with maximum differences of ∼10% suggesting more lightning downwind of non-tornadic cases. There are no significant differences in the distance of the tornadic versus non-tornadic cells from the TC center suggesting that these results are not an artifact of the normalized radial coordinate used. Previous studies have shown that the downwind edge is typically located in the direction of synoptic-scale deep-tropospheric vertical wind shear vector, which is coincident with the most favorable kinematic and thermodynamic environments in TCs (Molinari & Vollaro, 2008; Schenkel et al., 2020).

More broadly, flashes occur more often in most radii at $r_{cell} \geq 1$ for the tornadic subset indicating that the TC outer rainbands are more convectively active. Nonetheless, the number of flashes throughout the entire TC shows no relationship with the number of flashes associated with the tornadic or non-tornadic subset (not shown). Together, these results show that tornadic cells tend to be located further downwind of a stronger lightning maximum that may be embedded in TCs with more outer region lightning. Moreover, these differences are consistent with prior conceptual models showing that the strongest cells are often located on the downwind edge of the convective portion of TC rainbands suggesting this portion of the rainband is a region to watch in operations (Hence & Houze, 2008, 2012).

The broad-scale lightning maxima, shown in Figure 10, associated with tornadic and non-tornadic cells also propagates away from the TC center in the hours before and after cell occurrence. To demonstrate this, Figure 11 shows differences in the TC-relative distance between the cell and its associated flashes within a ±45° TC-relative azimuth of the cell before, during, and after cell occurrence. This plot shows the structure of the broader-scale lightning maximum while smoothing out the lightning associated with any given cell given their small spatial scale and short lifetime (McCaul, 1987; Spratt et al., 1997). The centroid of the flash maximum in the composites propagates at ∼7–8 m s^{-1} away from the TC center, similar to prior diagnosed phase speeds of TC rainbands

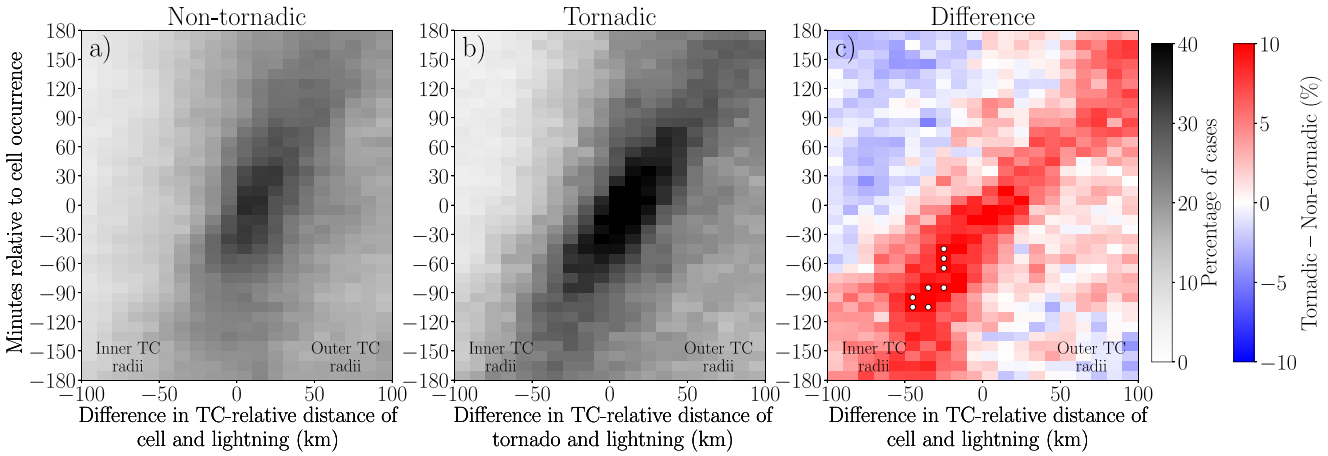

Figure 11. Percentage of cases with ≥1 ENTLN flashes in a joint histogram of difference in TC-relative distance of cells and lightning (km) versus minutes relative to the occurrence of (a) non-tornadic, (b) tornadic cells, and (c) their difference (tornadic-non-tornadic cells). All flashes within a ±45° TC-relative azimuth of the non-tornadic and tornadic cells are aggregated. White dots show bins with statistically significant percentage differences between the tornadic and non-tornadic subsets using a 10,000-sample bootstrap test with a false discovery rate of $\alpha = 0.1$ in panel (c).

(Li & Wang, 2012; May 1996). The speed and direction of propagation are also comparable with TC diurnal pulses (Ditchek, Molinari, et al., 2019; Dunion et al., 2014), although slower than the typical speed of the subset of pulses associated with lightning (Ditchek, Corbosiero, et al., 2019). However, the TC tornadic cases show more distinct propagation of a lightning maximum with maximum grid point differences of 12%, and significantly more cases with lightning radially inwards and before the tornado. These significant differences in flashes occurred nearly 2 hr before the time of the tornado. However, these differences are likely partially due to the differing subsets of TCs included in the tornadic and non-tornadic cell cases, given substantial differences in the radial propagation speed and the lack of significant differences when limiting the analysis to only those tornadic cells collocated with non-tornadic cells (not shown).

The location and magnitude of the broad-scale lightning maxima in Figure 10 varies with time in both the tornadic and non-tornadic cells, yielding long-lived, distinct differences in the TC-relative azimuth of the lightning maxima (as shown in Figure 12). Specifically, Figure 12 shows this as the differences in the TC-relative azimuth between each cell and its associated lightning before and after cell occurrence. While both subsets show local enhancements of lightning associated with the occurrence of the tornadic and non-tornadic subsets within the broader lightning maximum, there are also two regions of significant differences: (a) an enhanced percentage of cases with lightning upwind (i.e., in the direction opposing cyclonic TC winds) of the tornadic cell location beginning ∼2 hr before and (b) a suppressed percentage of cases with lightning downwind of the tornadic cell

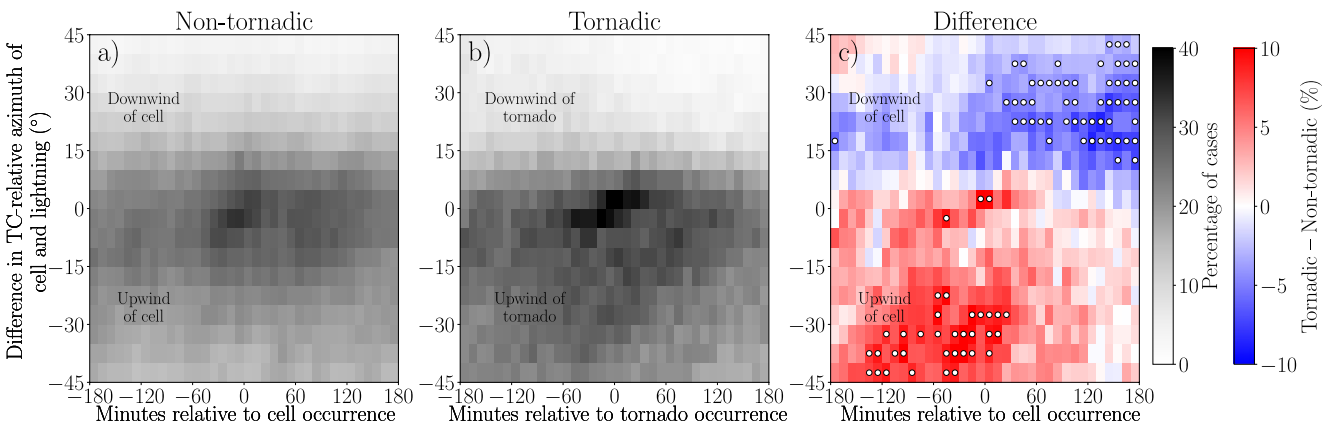

Figure 12. As in Figure 11, but for minutes relative to the tornadic or non-tornadic cell versus TC-relative azimuth (°). All flashes within a 100-km TC-relative distance of the tornadic or non-tornadic cell are aggregated.

location for 3 hr after tornado occurrence. These results are partially attributable to the broad-scale lightning maxima shifting further upwind in the non-tornadic cell subset with time compared to the tornadic cases. Moreover, there is a sharper reduction in the percentage of cases associated with lightning following tornadic cell occurrence relative to non-tornadic cases.

These results suggest that tornadic cells typically occur on the downwind edge of a persistent and stronger lightning maximum than non-tornadic cases. This maximum also propagates away from the TC center in the tornadic and non-tornadic subsets, while being advected less strongly around the TC center with time for tornadic cases. These patterns in lightning throughout the TC may be additional indicators of tornado occurrence along with flashes local to tornadic cells, especially when used with trends in low-level rotation and convergence from radar data (Edwards, 2012; Martinaitis, 2017). These results may also suggest that tornadic cells occur within TCs with more outer region convection than non-tornadic cases. The propagation speed and direction of these lightning maxima away from the TC center suggests that some tornadic cells may be embedded in rainbands associated with diurnal pulses, as implied in a case study of Hurricane Harvey (2017; Ditchek et al., 2020). The enhanced rightward deviant motion of TC tornadic cells compared to their non-tornadic counterparts may impart a component away from the TC, and may also contribute to the propagation of the lightning maximum away from the TC (Bunkers et al., 2014; Eastin & Link, 2009). However, the scale of the lightning maximum is well beyond the diameter of the largest TC tornadic cells (i.e., 20 km) suggesting that this is a secondary factor compared to differences in TC structure (Baker et al., 2009; Spratt et al., 1998).

4. Summary and Discussion

The present study investigated the lightning and radar characteristics of tornadic cells in landfalling TCs for comparison with TC non-tornadic and non-TC EF0–EF1 tornadic cells. Data from three lightning networks were used—the ENTLN, NLDN, and GLM. This study first examined differences in the number and location of flashes between tornadic and non-tornadic subsets in the immediate area surrounding their cells. Then this work examined how radar-derived velocity variables evolve before and during TC tornado occurrence for comparison with both TC non-tornadic and non-TC tornadic cases. Finally, differences in lightning throughout the TC before, during, and after the time of tornadic and non-tornadic cells were examined.

These results suggest that TC tornadic cells are not typically associated with lightning in the 10 min before the tornado. However, TC tornadic cases are associated with lightning more frequently than non-tornadic convection. The tornadic subset has a larger percentage of cases with >100 flashes in the 10 min before the tornadic or non-tornadic cell occurrence in the ENTLN, since this network can detect a larger percentage of IC and CG pulses compared to the NLDN and GLM. This analysis also showed strong variability in the number of tornadic and non-tornadic cells with ≥1 flash among TCs. This large variability may be associated with differences in the distance of tornadic and non-tornadic cells from the TC center among TCs as well as the intensity of the TC. These factors may also be proxies for other factors like TC outer size, especially since larger TCs tend to be associated with more tornadoes that occur farther from the TC center due to a broader set of TC radii with favorable kinematic environments (McCaul, 1991; Paredes et al., 2021). The location of flashes also differs strongly between the two subsets with lightning concentrated to the northeast of tornadic cells, whereas lightning is distributed more symmetrically around non-tornadic cells. Finally, analysis of flashes in the hour before the TC tornado showed no significant changes.

The radar characteristics of tornadic mesocyclones are typified by stronger 0.5°-elevation angle maximum azimuthal shear and minimum divergent shear associated with TC tornadic versus non-tornadic mesocyclones. Relative to non-TC tornadic mesocyclones, the radar variable distributions were shifted toward slightly weaker magnitudes for the TC tornadic subset, although these differences were very small especially compared to those between tornadic and non-tornadic mesocyclones in TCs. The stronger magnitude of radar-derived variables for non-TC tornadoes is consistent with its slightly stronger maximum damage-based velocities and smaller percentage of EF0 tornadoes relative to TC tornadoes mentioned previously. Trends in radar characteristics in the hour before the tornado show that the distributions of maximum azimuthal shear and minimum divergent shear are initially slightly narrower for TC tornadic mesocyclones compared to non-TC tornadic cases. However, the TC tornadic distribution broadens more rapidly thereafter for both radar quantities yielding only small differences at the time of the tornado between the two subsets. Last, there is no significant relationship between maximum azimuthal shear or minimum divergent shear with the number of flashes preceding and during TC tornadic and non-tornadic cells.

Analysis of lightning differences throughout the TC showed that tornadic cells are often located in the downwind edge of a broad-scale maximum in lightning. In contrast, TC non-tornadic cells are located in the middle of a weaker lightning maximum. The lightning maximum associated with TC tornadic cells showed a greater percentage of cases with flashes in the hours before cell occurrence. Both subsets showed that these lightning maxima propagated away from the TC over time. The TC-relative azimuthal location of these broad-scale lightning maximum remained more stationary for the tornadic cell cases relative to the non-tornadic subset in the hours before and after cell occurrence. Tornadic cases were also associated with a greater number of cases with lightning throughout most of the time before and after cell occurrence. Together, these factors yielded more lightning upwind and before tornadic cells, and a suppressed number of cases with lightning downwind and after.

In summary, this study suggests that radar-derived low-level rotation and convergence may be useful for discriminating between tornadic and non-tornadic cells in TCs than either lightning both local to cells and, more broadly, throughout the TC. These results also answer the motivating questions from the Introduction.

1. How do the frequency and location of lightning associated with tornadic and non-tornadic cells differ in TCs?
   TC tornadic cells are more likely associated with ≥1 flash, especially ≥100 flashes, in the 10 min before tornado occurrence that are more strongly concentrated to the northeast of the cell.
2. Does lightning increase before tornado occurrence?
   Most TC tornadic cells show no significant increases in the number of flashes in the hour before the tornado.
3. What differences exist in low-level rotation and convergence before tornado occurrence among TC and non-TC events compared to TC non-tornadic mesocyclones?
   Tornadic mesocyclones in TCs tend to have slightly weaker low-level rotation and convergence followed by more rapid increases during the hour before the tornado, such that there are small differences with non-TC tornadic mesocyclones during tornado occurrence.
4. Are there differences in lightning characteristics throughout the TC before, during, and after tornadic versus non-tornadic cell occurrence?
   TC tornadic cases are located further downwind of a lightning maximum compared to non-tornadic cases, with both subsets showing that these lightning maxima propagate away from the TC over time.

This analysis of the radar-based kinematic structure and lightning local to tornadic cells, along with their interrelationship, corroborates prior findings. The examination of the lightning differences throughout the TC in the hours surrounding tornado occurrence is one of the first. Rather than using a reduced "lightning jump" threshold for identifying TC tornadic cells from non-TC tornadic cases, these results suggest that lightning trends may not be useful for most cases, given the dearth of flashes in TCs, although further work is needed given the conclusions of prior work (C. J. Schultz et al., 2009, 2011). These results also more broadly inform a greater understanding of TC convective structure following landfall, which has been less intensively studied than the TC inner core before landfall. Future work is needed to understand how tornadic cell distance from the TC and TC intensity impact lightning or whether these are proxies for other factors (e.g., TC outer size). Additional work should investigate how these results change, if at all, when also including non-tornadic cells that do not occur at the same time as tornadic cells. These results also raise questions about what percentage of right-moving cells spawn tornadoes in landfalling TCs. Finally, this study motivates examining what relationship, if any, there is between tornadic cells and convectively active diurnal pulses in TCs (Ditchek, Corbosiero, et al., 2019; Ditchek et al., 2020).

Data Availability Statement

[Dataset]—TC track data were provided by the NHC and are available at https://www.nhc.noaa.gov/data/hurdat/hurdat2-1851-2022-050423.txt (Landsea & Franklin, 2013).

[Dataset]—TCTOR track data were provided by the SPC and are available at https://doi.org/10.5281/zenodo.8206537 (Edwards & Mosier, 2022).

[Dataset]—ONETOR track data were provided by the SPC and obtained from https://www.spc.noaa.gov/wcm/data/Actual_tornadoes.csv (Schaefer & Edwards, 1999).

[Dataset]—Single-radar data were curated by NCEI and available at Amazon as part of the NOAA Big Data Partnership at https://registry.opendata.aws/noaa-nexrad/ (Ansari et al., 2018).

[Software]—Non-tornadic and pre-tornadic data were constructed from single-radar data using the NOAA Weather and Climate Toolkit, available at https://www.ncdc.noaa.gov/wct/.

[Dataset]—Non-tornadic track data were constructed using NEXRAD single-radar reflectivity and radial velocity data (Sandmæl et al., 2023).

[Dataset]—Pre-tornadic track data were constructed from sequential scans of NEXRAD single-radar reflectivity and radial velocity data.

[Dataset]—ENTLN lightning data were provided by Earth Networks, and can be acquired for academic use by contacting Earth Networks at https://get.earthnetworks.com/contactus (Zhu et al., 2017).

[Dataset]—NLDN lightning data were provided by Vaisala, and can be acquired for academic use by contacting Vaisala at https://www.vaisala.com/en/digital-and-data-services/lightning (Murphy et al., 2021).

[Dataset]—GLM lightning data were provided by NCEI, and can be obtained at https://www.ncei.noaa.gov/access/metadata/landing-page/bin/iso?id=gov.noaa.ncdc:C01527 (Goodman et al., 2013).

[Software]—Azimuthal shear and divergent shear data were computed using Warning Decision Support System-Integrated Information, available at http://www.wdssii.org/download.shtml (Lakshmanan et al., 2007).

[Software]—All figures were made using Matplotlib, version 3.6.3, available under the Matplotlib license at https://matplotlib.org/ (Caswell et al., 2023; Hunter, 2007).

Acknowledgments

This work is generously supported by funding from the NOAA VORTEX-SE program, NSF AGS-2028151, and by the NOAA/Office of Oceanic and Atmospheric Research under the NOAA-University of Oklahoma Cooperative Agreement NA21OAR4320204, U.S. Department of Commerce. The statements, findings, conclusions, and recommendations herein are those of the authors and do not necessarily reflect the views of OU, CIWRO, NOAA, and NSF. We would like to thank Elizabeth DiGangi (ENI) and Scott Rudlosky (NOAA) for their help with data procurement. We would like to acknowledge critical and constructive comments from Roger Edwards (SPC), Martin Murphy (Vaisala), an anonymous reviewer, and Xiushu Qie (LAGEO). We would also like to thank feedback from Steven Martinaitis (CIWRO/NSSL), Matthew Flournoy (CIWRO/SPC), Addison Alford (NSSL), Anthony Reinhart (NSSL), Adrian Campbell (CIWRO/NSSL), and Robert Deal (NOAA/NWS). This work would not have been possible without TCTOR data from NOAA/NWS SPC, IBTrACS data from NOAA/NCDC, and lightning data from Earth Networks, Vaisala, and NOAA.

References

Adachi, T., & Mashiko, W. (2020). High temporal-spatial resolution observation of tornadogenesis in a shallow supercell associated with Typhoon Hagibis (2019) using phased array weather radar. *Geophysical Research Letters*, *47*(19), e2020GL089635. https://doi.org/10.1029/2020gl089635

Ansari, S., Del Greco, S., Kearns, E., Brown, O., Wilkins, S., Ramamurthy, M., et al. (2018). Unlocking the potential of NEXRAD data through NOAA's Big Data Partnership [Dataset]. Bulletin America Meteorology Social, *99*(1), 189–204. https://doi.org/10.1175/bams-d-16-0021.1

Bai, L., Meng, Z., Huang, L., Yan, L., Li, Z., Mai, X., et al. (2017). An integrated damage, visual, and radar analysis of the 2015 Foshan, Guangdong, EF3 tornado in China produced by the landfalling Typhoon Mujigae (2015). *Bulletin America Meteorology Social*, *98*(12), 2619–2640. https://doi.org/10.1175/bams-d-16-0015.1

Baker, A. K., Parker, M. D., & Eastin, M. D. (2009). Environmental ingredients for supercells and tornadoes within Hurricane Ivan. *Weather and Forecasting*, *24*(1), 223–244. https://doi.org/10.1175/2008waf2222146.1

Barnes, G., Zipser, E., Jorgensen, D., & Marks, F. (1983). Mesoscale and convective structure of a hurricane rainband. *Journal of the Atmospheric Sciences*, *40*(9), 2125–2137. https://doi.org/10.1175/1520-0469(1983)040<2125:macsoa>2.0.co;2

Barron, N. R., Didlake, A. C., Jr., & Reasor, P. D. (2022). Statistical analysis of convective updrafts in tropical cyclone rainbands observed by airborne Doppler radar. *Journal of Geophysical Research*, *127*(6), e2021JD035718. https://doi.org/10.1029/2021jd035718

Bateman, M., & Mach, D. (2020). Preliminary detection efficiency and false alarm rate assessment of the Geostationary Lightning Mapper on the GOES-16 satellite. *Journal of Applied Remote Sensing*, *14*(3), 032406. https://doi.org/10.1117/1.jrs.14.032406

Benjamini, Y., & Hochberg, Y. (1995). Controlling the false discovery rate: A practical and powerful approach to multiple testing. *Journal of the Royal Statistical Society*, *57*(1), 289–300. https://doi.org/10.1111/j.2517-6161.1995.tb02031.x

Bitzer, P. M., & Burchfield, J. C. (2016). Bayesian techniques to analyze and merge lightning locating system data. *Geophysical Research Letters*, *43*(24), 12605–12613. https://doi.org/10.1002/2016gl071951

Black, R. A., & Hallett, J. (1999). Electrification of the hurricane. *Journal of the Atmospheric Sciences*, *56*(12), 2004–2028. https://doi.org/10.1175/1520-0469(1999)056<2004:eoth>2.0.co;2

Black, R. A., & Hallett, J. (1986). Observations of the distribution of ice in hurricanes. *Journal of the Atmospheric Sciences*, *43*(8), 802–822. https://doi.org/10.1175/1520-0469(1986)043<0802:ootdoi>2.0.co;2

Bogner, P. B., Barnes, G. M., & Franklin, J. L. (2000). Conditional instability and shear for six hurricanes over the Atlantic Ocean. *Weather and Forecasting*, *15*(2), 192–207. https://doi.org/10.1175/1520-0434(2000)015<0192:ciasfs>2.0.co;2

Bruning, E. C., & MacGorman, D. R. (2013). Theory and observations of controls on lightning flash size spectra. *Journal of the Atmospheric Sciences*, *70*(12), 4012–4029. https://doi.org/10.1175/jas-d-12-0289.1

Bunkers, M. J., Barber, D. A., Thompson, R. L., Edwards, R., & Garner, J. (2014). Choosing a universal mean wind for supercell motion prediction. *Journal of Operational Meteorology*, *2*(11), 115–129. https://doi.org/10.15191/nwajom.2014.0211

Carroll-Smith, D. L., Dawson, L. C., & Trapp, R. J. (2019). High resolution real-data WRF modeling and verification of tropical cyclone tornadoes associated with Hurricane Ivan 2004. *E-Journal of Severe Storms Meteorology*, *14*(2), 1–36. https://doi.org/10.55599/ejssm.v14i2.72

Caswell, T. A., Lee, A., Droettboom, M., de Andrade, E. S., Hoffman, T., Klymak, J., & Kniazev, N. (2023). matplotlib/matplotlib: REL: v3.6.3 [Software]. Zenodo. https://zenodo.org/record/7527665

Cecil, D. J., Zipser, E. J., & Nesbitt, S. W. (2002). Reflectivity, ice scattering, and lightning characteristics of hurricane eyewalls and rainbands. Part I: Quantitative description. *Monthly Weather Review*, *130*(4), 769–784. https://doi.org/10.1175/1520-0493(2002)130<0769:risalc>2.0.co;2

Corbosiero, K., & Molinari, J. (2002). The effects of vertical wind shear on the distribution of convection in tropical cyclones. *Monthly Weather Review*, *130*(8), 2110–2123. https://doi.org/10.1175/1520-0493(2002)130<2110:teovws>2.0.co;2

Cummins, K. L., & Murphy, M. J. (2009). An overview of lightning locating systems: History, techniques, and data uses, with an in-depth look at the US NLDN. *IEEE Transactions on Electromagnetic Compatibility*, *51*(3), 499–518. https://doi.org/10.1109/temc.2009.2023450

Devanas, A., Gregoria, D., Kasper, K., & Santos, P. (2008). Tropical cyclone induced tornadoes associated with the formation of Tropical Storm Barry. *20th Conference on Climate Variability and Change* (p. JP.3).

Didlake, A. C., & Houze, R. A. (2009). Convective-scale downdrafts in the principal rainband of Hurricane Katrina (2005). *Monthly Weather Review*, *137*(10), 3269–3293. https://doi.org/10.1175/2009mwr2827.1

Ditchek, S. D., Corbosiero, K. L., Fovell, R. G., & Molinari, J. (2019). Electrically active tropical cyclone diurnal pulses in the Atlantic basin. *Monthly Weather Review*, *147*(10), 3595–3607. https://doi.org/10.1175/mwr-d-19-0129.1

Ditchek, S. D., Corbosiero, K. L., Fovell, R. G., & Molinari, J. (2020). Electrically active diurnal pulses in Hurricane Harvey (2017). *Monthly Weather Review*, *148*(6), 2283–2305. https://doi.org/10.1175/mwr-d-20-0022.1

Ditchek, S. D., Molinari, J., Corbosiero, K. L., & Fovell, R. G. (2019). An objective climatology of tropical cyclone diurnal pulses in the Atlantic basin. *Monthly Weather Review*, *147*(2), 591–605. https://doi.org/10.1175/mwr-d-18-0368.1

Dunion, J. P., Thorncroft, C. D., & Velden, C. S. (2014). The tropical cyclone diurnal cycle of mature hurricanes. *Monthly Weather Review*, *142*(10), 3900–3919. https://doi.org/10.1175/mwr-d-13-00191.1

Eastin, M. D., & Link, M. C. (2009). Miniature supercells in an offshore outer rainband of Hurricane Ivan (2004). *Monthly Weather Review*, *137*(7), 2081–2104. https://doi.org/10.1175/2009mwr2753.1

Edwards, R. (2010). Tropical cyclone tornado records for the modernized National Weather Service era. In *Proceedings of 25th Conference on Severe Local Storms* (p. P3.1).

Edwards, R. (2012). Tropical cyclone tornadoes: A review of knowledge in research and prediction. *E-Journal of Severe Storms Meteorology*, *7*(6), 1–61. https://doi.org/10.55599/ejssm.v7i6.42

Edwards, R., Dean, A. R., Thompson, R. L., & Smith, B. T. (2012). Convective modes for significant severe thunderstorms in the contiguous United States. Part III: Tropical cyclone tornadoes. *Weather and Forecasting*, *27*(6), 1507–1519. https://doi.org/10.1175/waf-d-11-00117.1

Edwards, R., LaDue, J. G., Ferree, J. T., Scharfenberg, K., Maier, C., & Coulbourne, W. L. (2013). Tornado intensity estimation: Past, present, and future. *Bulletin America Meteorology Social*, *94*(5), 641–653. https://doi.org/10.1175/bams-d-11-00006.1

Edwards, R., & Mosier, R. M. (2022). Over a quarter century of TCTOR: Tropical cyclone tornadoes in the WSR-88D era [Dataset]. *Proceedings of 30th Conference on Severe Local Storms, Santa Fe, NM* (p. 171).

Edwards, R., & Pietrycha, A. (2006). Archetypes for surface baroclinic boundaries influencing tropical cyclone tornado occurrence. *23rd Conference on Severe Local Storms, St. Louis, MO*. (p. P8.2).

Emanuel, K. (1986). An air-sea interaction theory for tropical cyclones. Part I: Steady-state maintenance. *Journal of the Atmospheric Sciences*, *43*(6), 585–604. https://doi.org/10.1175/1520-0469(1986)043<0585:aasitf>2.0.co;2

Goodman, S. J., Blakeslee, R. J., Koshak, W. J., Mach, D., Bailey, J., Buechler, D., et al. (2013). The GOES-R geostationary lightning mapper (GLM) [Dataset]. Atmospheric Research, *125*, 34–49. https://doi.org/10.1016/j.atmosres.2013.01.006

Green, B. W., Zhang, F., & Markowski, P. (2011). Multiscale processes leading to supercells in the landfalling outer rainbands of Hurricane Katrina (2005). *Weather and Forecasting*, *26*(6), 828–847. https://doi.org/10.1175/waf-d-10-05049.1

Hence, D. A., & Houze, R. A. (2008). Kinematic structure of convective-scale elements in the rainbands of Hurricanes Katrina and Rita (2005). *Journal of Geophysical Research*, *113*(D15), D15108. https://doi.org/10.1029/2007jd009429

Hence, D. A., & Houze, R. A. (2012). Vertical structure of tropical cyclone rainbands as seen by the TRMM precipitation radar. *Journal of the Atmospheric Sciences*, *69*(9), 2644–2661. https://doi.org/10.1175/jas-d-11-0323.1

Hill, E., Malkin, W., & Schulz, W. (1966). Tornadoes associated with cyclones of tropical origin—Practical features. *Journal of Applied Meteorology and Climatology*, *5*(6), 745–763. https://doi.org/10.1175/1520-0450(1966)005<0745:tawcot>2.0.co;2

Homeyer, C. R., Sandmæl, T. N., Potvin, C. K., & Murphy, A. M. (2020). Distinguishing characteristics of tornadic and nontornadic supercell storms from composite mean analyses of radar observations. *Monthly Weather Review*, *148*(12), 5015–5040. https://doi.org/10.1175/mwr-d-20-0136.1

Houze, R. A. (2010). Clouds in tropical cyclones. *Monthly Weather Review*, *138*(2), 293–344. https://doi.org/10.1175/2009mwr2989.1

Hunter, J. D. (2007). Matplotlib: A 2D graphics environment [Software]. Computer Science and Engineering, *9*(3), 90–95. https://doi.org/10.1109/MCSE.2007.55

Jones, T. A., Skinner, P., Yussouf, N., Knopfmeier, K., Reinhart, A., & Dowell, D. (2019). Forecasting high-impact weather in landfalling tropical cyclones using a Warn-on-Forecast system. *Bulletin America Meteorology Social*, *100*(8), 1405–1417. https://doi.org/10.1175/bams-d-18-0203.1

Knapp, K. R., Kruk, M. C., Levinson, D. H., Diamond, H. J., & Neumann, C. J. (2010). The International Best Track Archive for Climate Stewardship (IBTrACS) unifying tropical cyclone data [Dataset]. Bulletin America Meteorology Social, *91*(3), 363–376. https://doi.org/10.1175/2009bams2755.1

Lakshmanan, V., Smith, T., Stumpf, G., & Hondl, K. (2007). The warning decision support system–integrated information [Software]. Weather and Forecasting, *22*(3), 596–612. https://doi.org/10.1175/waf1009.1

Landsea, C. W., & Franklin, J. L. (2013). Atlantic hurricane database uncertainty and presentation of a new database format [Dataset]. Monthly Weather Review, *141*(10), 3576–3592. https://doi.org/10.1175/mwr-d-12-00254.1

Li, Q., & Wang, Y. (2012). Formation and quasi-periodic behavior of outer spiral rainbands in a numerically simulated tropical cyclone. *Journal of the Atmospheric Sciences*, *69*(3), 997–1020. https://doi.org/10.1175/2011jas3690.1

Liu, C., Sloop, C., & Heckman, S. (2014). Application of lightning in predicting high impact weather. In *Obs/imo/teco-2014, wmo*. Retrieved from https://www.wmo.int/pages/prog/www/IMOP/publications/IOM-116_TECO-2014/Session%201/O1_Liu_Lightning_application_DTA.pdf

MacGorman, D. (1993). Lightning in tornadic storms: A review. In C. R. Church (Ed.), *The tornado: Its structure, dynamics, prediction, and hazards* (pp. 173–182). AGU.

Mahalik, M. C., Smith, B. R., Elmore, K. L., Kingfield, D. M., Ortega, K. L., & Smith, T. M. (2019). Estimates of gradients in radar moments using a linear least squares derivative technique. *Weather and Forecasting*, *34*(2), 415–434. https://doi.org/10.1175/waf-d-18-0095.1

Marchand, M., Hilburn, K., & Miller, S. D. (2019). Geostationary Lightning Mapper and Earth Networks lightning detection over the contiguous United States and dependence on flash characteristics. *Journal of Geophysical Research*, *124*(21), 11552–11567. https://doi.org/10.1029/2019jd031039

Marks, F. D., & Houze, R. A. (1987). Inner core structure of Hurricane Alicia from airborne Doppler radar observations. *Journal of the Atmospheric Sciences*, *44*(9), 1296–1317. https://doi.org/10.1175/1520-0469(1987)044<1296:icsoha>2.0.co;2

Martinaitis, S. M. (2017). Radar observations of tornado-warned convection associated with tropical cyclones over Florida. *Weather and Forecasting*, *32*(1), 165–186. https://doi.org/10.1175/waf-d-16-0105.1

May, P. T. (1996). The organization of convection in the rainbands of Tropical Cyclone Laurence. *Monthly Weather Review*, *124*(5), 807–815. https://doi.org/10.1175/1520-0493(1996)124<0807:toocit>2.0.co;2

McCaul, E. W. (1987). Observations of the hurricane "Danny" tornado outbreak of 16 August 1985. *Monthly Weather Review*, *115*(6), 1206–1223. https://doi.org/10.1175/1520-0493(1987)115<1206:oothto>2.0.co;2

McCaul, E. W. (1991). Buoyancy and shear characteristics of hurricane-tornado environments. *Monthly Weather Review*, *119*(8), 1954–1978. https://doi.org/10.1175/1520-0493(1991)119<1954:bascoh>2.0.co;2

McCaul, E. W., Buechler, D. E., Goodman, S. J., & Cammarata, M. (2004). Doppler radar and lightning network observations of a severe outbreak of tropical cyclone tornadoes. *Monthly Weather Review*, *132*(7), 1747–1763. https://doi.org/10.1175/1520-0493(2004)132<1747:dralno>2.0.co;2

McCaul, E. W., & Weisman, M. L. (1996). Simulations of shallow supercell storms in landfalling hurricane environments. *Monthly Weather Review*, *124*(3), 408–429. https://doi.org/10.1175/1520-0493(1996)124<0408:sosssi>2.0.co;2

Molinari, J., Moore, P., & Idone, V. (1999). Convective structure of hurricanes as revealed by lightning locations. *Monthly Weather Review*, *127*(4), 520–534. https://doi.org/10.1175/1520-0493(1999)127<0520:csohar>2.0.co;2

Molinari, J., Romps, D. M., Vollaro, D., & Nguyen, L. (2012). CAPE in tropical cyclones. *Journal of the Atmospheric Sciences*, *69*(8), 2452–2463. https://doi.org/10.1175/jas-d-11-0254.1

Molinari, J., & Vollaro, D. (2008). Extreme helicity and intense convective towers in Hurricane Bonnie. *Monthly Weather Review*, *136*(11), 4355–4372. https://doi.org/10.1175/2008mwr2423.1

Morotomi, K., Shimamura, S., Kobayashi, F., Takamura, T., Takano, T., Higuchi, A., & Iwashita, H. (2020). Evolution of a tornado and debris ball associated with Super Typhoon Hagibis 2019 observed by x-band phased array weather radar in Japan. *Geophysical Research Letters*, *47*(24), e2020GL091061. https://doi.org/10.1029/2020gl091061

Murphy, M. J., Cramer, J. A., & Said, R. K. (2021). Recent history of upgrades to the US National Lightning Detection Network [Dataset]. Journal of Atmospheric and Oceanic Technology, *38*(3), 573–585. https://doi.org/10.1175/jtech-d-19-0215.1

NOAA/National Weather Service NWS. (1950). Storm Events Database (Tech. Rep.). Retrieved from https://www.ncdc.noaa.gov/stormevents/

NOAA National Weather Service Operations Center. (1991). *NOAA Next Generation Radar (NEXRAD) level 2 base data*. NOAA National Centers for Environmental Information.

Novlan, D. J., & Gray, W. M. (1974). Hurricane-spawned tornadoes. *Monthly Weather Review*, *102*(7), 476–488. https://doi.org/10.1175/1520-0493(1974)102<0476:hst>2.0.co;2

Nowotarski, C. J., Spotts, J., Edwards, R., Overpeck, S., & Woodall, G. R. (2021). Tornadoes in Hurricane Harvey. *Weather and Forecasting*, *36*(5), 1589–1609. https://doi.org/10.1175/waf-d-20-0196.1

Orville, R. E. (2008). Development of the national lightning detection network. *Bulletin America Meteorology Social*, *89*(2), 180–190. https://doi.org/10.1175/bams-89-2-180

Paredes, M., Schenkel, B. A., Edwards, R., & Coniglio, M. (2021). Tropical cyclone outer size impacts the number and location of tornadoes. *Geophysical Research Letters*, *48*(24), e2021GL095922. https://doi.org/10.1029/2021gl095922

Rappaport, E. N. (2014). Fatalities in the United States from Atlantic tropical cyclones: New data and interpretation. *Bulletin America Meteorology Social*, *95*(3), 341–346. https://doi.org/10.1175/bams-d-12-00074.1

Ray, P. S., Macgorman, D. R., Rust, W. D., Taylor, W. L., & Rasmussen, L. W. (1987). Lightning location relative to storm structure in a supercell storm and a multicell storm. *Journal of Geophysical Research*, *92*(D5), 5713–5724. https://doi.org/10.1029/jd092id05p05713

Ringhausen, J. S., & Bitzer, P. M. (2021). An in-depth analysis of lightning trends in Hurricane Harvey using satellite and ground-based measurements. *Journal of Geophysical Research*, *126*(7), e2020JD032859. https://doi.org/10.1029/2020jd032859

Rios-Berrios, R., & Torn, R. D. (2017). Climatological analysis of tropical cyclone intensity changes under moderate vertical wind shear. *Monthly Weather Review*, *145*(5), 1717–1738. https://doi.org/10.1175/mwr-d-16-0350.1

Rudlosky, S. D., Goodman, S. J., Virts, K. S., & Bruning, E. C. (2019). Initial geostationary lightning mapper observations. *Geophysical Research Letters*, *46*(2), 1097–1104. https://doi.org/10.1029/2018gl081052

Samsury, C. E., & Orville, R. E. (1994). Cloud-to-ground lightning in tropical cyclones: A study of hurricanes Hugo (1989) and Jerry (1989). *Monthly Weather Review*, *122*(8), 1887–1896. https://doi.org/10.1175/1520-0493(1994)122<1887:ctglit>2.0.co;2

Sandmæl, T. N., Homeyer, C. R., Bedka, K. M., Apke, J. M., Mecikalski, J. R., & Khlopenkov, K. (2019). Evaluating the ability of remote sensing observations to identify significantly severe and potentially tornadic storms. *Journal of Applied Meteorology and Climatology*, *58*(12), 2569–2590. https://doi.org/10.1175/jamc-d-18-0241.1

Sandmæl, T. N., Smith, B., Reinhart, A., Schick, I., Ake, M., Madden, J., et al. (2023). The tornado potential algorithm: A machine-learning probability-based tornadic circulation detection algorithm [Dataset]. Weather and Forecasting, *38*(3), 445–466. https://doi.org/10.1175/waf-d-22-0123.1

Saunders, C., & Peck, S. (1998). Laboratory studies of the influence of the rime accretion rate on charge transfer during crystal/graupel collisions. *Journal of Geophysical Research*, *103*(D12), 13949–13956. https://doi.org/10.1029/97jd02644

Schaefer, J., & Edwards, R. (1999). The SPC tornado/severe thunderstorm database [Dataset]. *Preprints, 11th Conference on Applied Climatology, Dallas, TX*, (pp. 215–220).

Schenkel, B. A., Edwards, R., & Coniglio, M. (2020). A climatological analysis of ambient deep-tropospheric vertical wind shear impacts upon tornadic supercells in tropical cyclones. *Weather and Forecasting*, *35*(5), 2033–2059. https://doi.org/10.1175/waf-d-19-0220.1

Schneider, D., & Sharp, S. (2007). Radar signatures of tropical cyclone tornadoes in central North Carolina. *Weather Forecasting*, *22*(2), 278–286. https://doi.org/10.1175/waf992.1

Schultz, C. J., Petersen, W. A., & Carey, L. D. (2009). Preliminary development and evaluation of lightning jump algorithms for the real-time detection of severe weather. *Journal of Applied Meteorology and Climatology*, *48*(12), 2543–2563. https://doi.org/10.1175/2009jamc2237.1

Schultz, C. J., Petersen, W. A., & Carey, L. D. (2011). Lightning and severe weather: A comparison between total and cloud-to-ground lightning trends. *Weather and Forecasting*, *26*(5), 744–755. https://doi.org/10.1175/waf-d-10-05026.1

Schultz, L. A., & Cecil, D. J. (2009). Tropical cyclone tornadoes, 1950–2007. *Monthly Weather Review*, *137*(10), 3471–3484. https://doi.org/10.1175/2009mwr2896.1

Smith, T. M., & Elmore, K. L. (2004). The use of radial velocity derivatives to diagnose rotation and divergence. In *11th Conference on Aviation, Range, and Aerospace*. Hyannis.

Spratt, S. M., Sharp, D. W., & Hodanish, S. J. (1998). Observed relationships between total lightning information and Doppler radar data during two recent tropical cyclone tornado events in Florida. *Proceedings of 19th Conference on Severe Local Storms, Minneapolis, MN*, (pp. 659–662).

Spratt, S. M., Sharp, D. W., Welsh, P., Sandrik, A., Alsheimer, F., & Paxton, C. (1997). A WSR-88D assessment of tropical cyclone outer rainband tornadoes. *Weather and Forecasting*, *12*(3), 479–501. https://doi.org/10.1175/1520-0434(1997)012<0479:awaotc>2.0.co;2

Stough, S. M., Carey, L. D., Schultz, C. J., & Bitzer, P. M. (2017). Investigating the relationship between lightning and mesocyclonic rotation in supercell thunderstorms. *Weather and Forecasting*, *32*(6), 2237–2259. https://doi.org/10.1175/waf-d-17-0025.1

Suzuki, O., Niino, H., Ohno, H., & Nirasawa, H. (2000). Tornado-producing mini supercells associated with Typhoon 9019. *Monthly Weather Review*, *128*(6), 1868–1882. https://doi.org/10.1175/1520-0493(2000)128<1868:tpmsaw>2.0.co;2

Takahashi, T. (1978). Riming electrification as a charge generation mechanism in thunderstorms. *Journal of the Atmospheric Sciences*, *35*(8), 1536–1548. https://doi.org/10.1175/1520-0469(1978)035<1536:reaacg>2.0.co;2

Wilks, D. S. (2016). The stippling shows statistically significant grid points": How research results are routinely overstated and overinterpreted, and what to do about it. *Bulletin America Meteorology Social*, *97*(12), 2263–2273. https://doi.org/10.1175/bams-d-15-00267.1

Williams, E. R. (2001). The electrification of severe storms. In C. Doswell (Ed.), *Severe convective storms* (pp. 527–561). American Meteorological Society.

Williams, E. R., Boldi, B., Matlin, A., Weber, M., Hodanish, S., Sharp, D., et al. (1999). The behavior of total lightning activity in severe Florida thunderstorms. *Atmospheric Research*, *51*(3–4), 245–265. https://doi.org/10.1016/s0169-8095(99)00011-3

Willoughby, H., Clos, J., & Shoreibah, M. (1982). Concentric eyewalls, secondary wind maxima, and the evolution of the hurricane vortex. *Journal of the Atmospheric Sciences*, *39*(2), 395–411. https://doi.org/10.1175/1520-0469(1982)039<0395:cewswm>2.0.co;2

Willoughby, H., Jorgensen, D., Black, R., & Rosenthal, S. (1985). Project STORMFURY: A scientific chronicle 1962–1983. *Bulletin America Meteorology Social*, *66*(5), 505–514. https://doi.org/10.1175/1520-0477(1985)066<0505:psasc>2.0.co;2

Zhang, D., & Cummins, K. L. (2020). Time evolution of satellite-based optical properties in lightning flashes, and its impact on GLM flash detection. *Journal of Geophysical Research*, *125*(6). https://doi.org/10.1029/2019jd032024

Zhu, Y., Rakov, V., Tran, M., Stock, M., Heckman, S., Liu, C., et al. (2017). Evaluation of ENTLN performance characteristics based on the ground truth natural and rocket-triggered lightning data acquired in Florida [Dataset]. Journal of Geophysical Research, *122*(18), 9858–9866. https://doi.org/10.1002/2017jd027270